Arabidopsis thaliana Root Responses to Cd Exposure: insights into root tip-specific changes and the role of HY5 in limiting Cd accumulation and promoting tolerance

Ludwig Richtmann[1,2*], Noémie Thiébaut[2,3*], Santiago Prochetto[2,3*], Manon Sarthou[3], Stéphanie Boutet[4], Marc Hanikenne[3], Stephan Clemens[1] ✉ and Nathalie Verbruggen[2] ✉

[1] Department of Plant Physiology, University of Bayreuth, 95447 Bayreuth, Germany

[2] Laboratory of Plant Physiology and Molecular Genetics, Université libre de Bruxelles, 1050 Brussels, Belgium

[3] InBioS-PhytoSystems, Translational Plant Biology, University of Liège, 4000 Liège, Belgium

[4] Institut Jean-Pierre Bourgin, Université Paris-Saclay, INRAE, AgroParisTech, 78000, Versailles, France

* These authors contributed equally to this work

✉ Corresponding authorship is shared between Stephan Clemens (stephan.clemens@uni-bayreuth.de) and Nathalie Verbruggen (Nathalie.Verbruggen@ulb.be)

Word count: 8462 words

Summary: 212 words

Introduction: 1097 words

Materials and Methods: 1029 words

Results: 2827 words

Discussion: 2249 words

Figures: 6 (all in colour)

Supporting information: 12 supporting figures, 7 supporting tables.

Significance Statement

This study provides new insights into the regulatory networks governing root responses to Cd, highlighting HY5 as a central player in Cd tolerance mechanisms. These findings enhance our understanding of HY5's role in metal homeostasis and stress adaptation in plants

Summary

Cadmium (Cd) is a major environmental pollutant with high toxicity. While Cd exposure reduces root growth, its specific impact on the root meristem and differentiating parts remains poorly understood. This study investigates the spatial and temporal responses of *Arabidopsis thaliana* roots to Cd stress by dividing roots into root tips (RT) and remaining roots (RR) and employing transcriptomic, ionomic, and metabolomic analyses.

Cd exposure altered mineral profiles, with RT accumulating less Cd but showing distinct changes in other elements compared to RR. Metabolomic analysis revealed root part-specific changes in phytochelatins, flavonoids, and glucosinolates. Transcriptomic data highlighted constitutive differences between RT and RR, reflecting functional specialization; alongside Cd-induced root part-specific and time-dependent transcriptional responses, including modulation of Fe-related genes. Phenotypic validation identified ELONGATED HYPOCOTYL 5 (HY5) as a key regulator limiting Cd accumulation and promoting tolerance, as *hy5* mutants exhibited increased Cd sensitivity and accumulation. Additionally, mutants of genes regulated by HY5 like xyloglucan endotransglucosylase/hydrolase genes (*XTH*) and *MYB12* also showed altered root growth under Cd stress, implicating cell wall remodeling and flavonoid biosynthesis in Cd responses.

This study provides a comprehensive understanding of Cd's impact on root growth, revealing spatial and temporal mechanisms and highlighting HY5's role in Cd tolerance, thereby advancing our knowledge of plant responses to trace metal excess.

Keywords

Metal homeostasis, Cadmium, RNA sequencing, Flavonoids, ICP, ELONGATED HYPOCOTYL 5 (HY5), *Arabidopsis thaliana,* Root tip.

Introduction

In natural environments, plant roots encounter diverse edaphic conditions and are confronted with variations in soil texture, water saturation, pH levels, salinity or nutrient availability. A variety of metal ions are required as macro- (Ca, K, Mg) or micronutrients (Fe, Cu, Co, Mn, Mo, Ni, Zn) and their availabilities in habitats nearly always deviate from optimal conditions (Lin & Aarts, 2012; Kumar *et al.*, 2021). Therefore, plants need a tightly regulated metal homeostasis network in order to handle either deficiencies or excess of metals, with the latter potentially causing toxicity. In addition to essential nutrients, metals such as cadmium (Cd) are present in soil as environmental contaminants, as they are not essential for plant growth and can be highly toxic (Lin & Aarts, 2012; Haider *et al.*, 2021). As a metal with known carcinogenic potential, the presence of Cd in agricultural soils and subsequent uptake by crops additionally represents a substantial threat to human health and motivates studies on its interaction with plants (Clemens *et al.*, 2013; Rahim *et al.*, 2022).

Plant root responses to maintain elemental homeostasis in challenging soil conditions can be broadly categorized into two general types. On the one hand, acclimatization to such environmental conditions can occur through developmental plasticity. For instance, *Arabidopsis thaliana* seedlings exhibit notable morphological alterations when grown under varying phosphate (P_i) availability. These involve changes in root system architecture such as the inhibition of primary root growth and enhanced elongation of the lateral roots and root hairs (Ren *et al.*, 2023). On the other hand, plants acclimatize to soil environments by modulating molecular networks that regulate uptake, transport, and storage of metals and other nutrients. For instance, in response to iron (Fe) deficiency, the transcriptional upregulation of central Fe uptake genes such as *IRT1* and *FRO2* relies on the formation of heterodimeric complexes between FIT and the group Ib basic helix-loop-helix (bHLH) transcription factors bHLH38 and bHLH39 (Riaz & Guerinot, 2021).

Similarly, exposure to Cd triggers a complex response in plants. The most prominent developmental consequence of Cd exposure is a reduction of growth in both above- and below-ground organs. This is the result of diverse toxicity mechanisms including the inhibition of enzymes, lipid peroxidation, overproduction of reactive oxygen species (ROS), induction of DNA damage and reduction of photosynthetic activity (Lin & Aarts, 2012; Haider *et al.*, 2021). To mitigate toxic effects upon Cd entry into the plant, the presence of efficient detoxification mechanisms is crucial. This is exemplified by the extreme Cd hypersensitivity of the *cad1-3* mutant, which lacks a functional Phytochelatin Synthase 1 (AtPCS1). The mutation strongly impairs its ability to synthesize metal-chelating phytochelatins (PCs), which, together with vacuolar sequestration of PC-Cd complexes, is a key mechanism to cope with metals such as Cd (Howden *et al.*, 1995; Lin & Aarts, 2012).

Besides these toxicity mechanisms, Cd is known to interfere with the homeostasis of essential elements, as illustrated by its intricate relationship with Fe acquisition (Wu *et al.*, 2012; Zhai *et al.*, 2014; Hanikenne et al., 2021; Zhou *et al.*, 2021; Wang *et al.*, 2023). Indeed, Cd exposure was shown to result in a reduction of root Fe content and the activation of Fe-deficiency responses (Lešková *et al.*, 2017). At least in part, the connection between Cd and Fe homeostasis may be attributable to the shared uptake pathways of the two metals. For instance, multiple studies suggest that, in *A. thaliana*, IRT1, a member of the ZIP (ZRT- and IRT-like proteins) family, plays a significant role in Cd uptake (Connolly *et al.*, 2002; Vert *et al.*, 2002; Fan *et al.*, 2014; Ismael *et al.*, 2019). Additionally, in the hypertolerant species *Arabidopsis halleri*, the Zn transporter ZIP6 was shown to be a Cd uptake transporter (Spielmann *et al.*, 2020). Besides ZIP family proteins, a significant contribution to Cd uptake under low nitrate conditions was demonstrated for the nitrate transporter NRT2.1 (Guan *et al.*, 2021). Furthermore, there is evidence for a major role of the manganese (Mn) and Fe transporter NRAMP5 in Cd uptake in rice (Ishimaru *et al.*, 2012; Clemens *et al.*, 2013).

Due to the abovementioned toxicity mechanisms, elevated Cd concentrations in the rhizosphere affect many aspects of root anatomy such as lateral root emergence (Wang *et al.*, 2021), root thickness (Lux *et al.*, 2011), root hair density (Bahmani *et al.*, 2022) and primary root growth. The latter depends on the tissues in the root apex: the root apical meristem (RAM), where cells undergo mitotic divisions, and the elongation/differentiation zone, where they expand to their final size and differentiate to achieve tissue-specific characteristics. Optimal root growth depends on meristem maintenance, which represents a tight balance between division and elongation/differentiation rates (Perilli *et al.*, 2012).

This balance is regulated, among others, by the two phytohormones auxin and cytokinin and the cellular response to their distribution in the root plays a critical role for the developmental characteristics in the different zones of the root apex (Dello Ioio *et al.*, 2007; Růžička *et al.*, 2009; Perilli *et al.*, 2010; Jia *et al.*, 2023; Tao *et al.*, 2024). Independently of auxin and cytokinin hormonal signaling, the developmental processes in the root tip are controlled by the distribution of reactive oxygen species (ROS). Proliferation and differentiation rates depend on a gradient between superoxide ions ($O_2^{\bullet -}$) and hydrogen peroxide (H_2O_2) (Tsukagoshi *et al.*, 2010; Wells *et al.*, 2010; Mase & Tsukagoshi, 2021).

Several studies have addressed the impact of Cd on the root apex of *A. thaliana*, examining disruptions in the auxin/cytokinin hormonal balance (Yuan & Huang, 2016; Bruno *et al.*, 2017; Leonardo *et al.*, 2021) or the effects on the cell cycle (Cui *et al.*, 2017). However, the effects of metal stress on the molecular networks regulating root growth and nutrient homeostasis have not been comprehensively examined.

In this study we showed that Cd accumulation was lower in the root tip (RT) than in the remaining root (RR), accompanied by distinct transcriptomic and metabolomic responses between the two root parts. Notably, our analyses highlighted a specific involvement of the transcription factor ELONGATED HYPOCOTYL 5 (HY5) in multiple aspects of the RT response to Cd, as reflected in both the transcriptomic and the metabolomic analyses. Indeed, several observations support the diverse roles of HY5 in limiting Cd accumulation and promoting Cd tolerance: (i) the Cd hypersensitivity of *hy5* mutants; (ii) the root growth reduction under Cd treatment of *myb12, xth26* and *hrg2* mutants, corresponding to genes known to be regulated by HY5 and involved in flavonoid biosynthesis, cell wall structure and ROS homeostasis, respectively; (iii) the elevated cellular Cd levels in *hy5*; and (iv) the increased GSH and PC levels in *hy5* under Cd exposure.

Materials & Methods

Plant material & growth conditions

A. thaliana (Col-0) seeds were surface sterilized by rinsing 3 min with 70% ethanol and 2 min with 2% bleach. Upon 3 washing steps with sterile H_2O, the seeds were suspended in 0.1% (w/v) sterile agar. All seeds were sown on nylon meshes and stratified (4°C, 2 days).

Plants were grown vertically on agar plates with Hoagland medium (1.5 mM $Ca(NO_3)_2$, 0. 28 mM KH_2PO_4, 0.75 mM $MgSO_4$, 1.25 mM KNO_3, 0.5 µM $CuSO_4$, 1 µM $ZnSO_4$, 5 µM $MnSO_4$, 25 µM H_3BO_3, 0.1 µM Na_2MoO_4, 50 µM KCl, 10 µM Fe-HBED, 3 mMMES, 1% (w/v) sucrose, 0.8% (w/v) agar (M-type, Sigma), pH 5.7) in a CLF Plant Climatics GroBank under long day light conditions (16 h light, 21°C, 100 PAR/8 h dark, 18°C). Fe-deficiency assays were conducted by adding 75 µM FerroZine. The mutant lines used were SALK_066689C (*xth20)*, SALK_042683C (*xth26)*, SALK_001585 (*cyp82c4),* GK_578C04 *(hrg1),* GK_772A03 *(hrg2)*, GABI DUPLO 1202/1a1.16.1 *(elip1-elip2,* NASC ID N2103098), *myb12-1-f* (Mehrtens *et al.*, 2005), SALK_0966551C (herein called *hy5_1)* and *hy5_215* (Oyama *et al.*, 1997).

ICP-MS

A preliminary experiment was conducted to determine the Cd concentration inhibiting root growth by 50% after one week of treatment. Based on these results, a concentration of 25 µM $CdCl_2$ was selected for further experiments. Seven-day-old seedlings were transferred to the Cd-contaminated medium, and samples were collected at 24 h and 48 h post-transfer. Plants were desorbed prior to ICP analysis, washed twice in a desorption solution [(5 mM $CaCl_2$, 1 mM MES, pH 5.7), 10 min, 4°C] and twice in distilled water (5 min, 4°C). RT samples were collected by separating ~2 mm RT from the RR as in Thiébaut *et al.*, (2024). Dry root material was weighed into polytetrafluoroethylene (PTFE) digestion tubes and concentrated nitric acid (0.5 mL, 67-69%) was added to each tube. After 4 h incubation, samples were

digested under pressure using a high-performance microwave reactor (Ultraclave 4, MLS). Digested samples were transferred to Greiner centrifuge tubes and diluted with deionized water. Elemental analysis was performed using inductively coupled plasma - mass spectrometry (Sector Field High Resolution (HR)-ICP-MS, ELEMENT 2, Thermo Fisher Scientific), coupled with a a SC-2 DX Autosampler (ESI, Elemental Scientific). A 6-point external calibration curve was set from a certified multiple standards solution (Bernd Kraft). The elements rhodium (Rh) and germanium (Ge) were infused online and used as internal standards.

Metabolomic analysis

For untargeted metabolomic analysis, plants were grown as described above. 48 h after transferring seedlings, RT and RR samples were taken by cutting and collecting similar sized pieces (~2 mm) of RT and RR (at ~mid-length of the primary root) as inThiébaut *et al.* 2024). Extraction and LC-MS/MS analysis of polar/semipolar primary and specialized metabolites from root material was done as described in Boutet *et al.*, (2022). Relative metabolite quantifications were normalized to the total metabolite count of each sample. Statistical analysis was done by fitting a linear model to $\log_2$ transformed metabolite data with limma and applying empirical Bayes moderation of the linear model fit. Features were considered as significant DAFs (differentially abundant features) when $|\log_2$ fold change$| > 1$ and $p_{adj} \leq 0.05$. For better comparison of metabolites between RR and RT, metabolite concentrations were normalized to the total metabolite count in each sample.

RNA isolation, cDNA synthesis & RNA-Sequencing

Seedlings were grown for 7 d on control medium before being transferred to Cd contaminated medium (25 µM). 24 h and 48 h after transferring seedlings, samples were collected by cutting RT (~2 mm from the apex), as in (Thiébaut *et al. 2024*). From each plate, the RR after cutting were also collected. RNA isolation was done with a Maxwell 16 device (Promega) using the Maxwell RSC Plant RNA Kit. This method isolates total RNA using cellulose-based paramagnetic particles and includes a DNAse I-treatment.

RNA quality and concentration were measured with an Agilent 2100 Bioanalyzer Expert using the Agilent Nano 6000 Kit. Library preparation was done with the TruSeq Stranded mRNA Sample Preparation Kit, using 1 µg of RNA as starting material. Library quality was assessed with a QIAxcel screening kit. Quantification, dilution and pooling of the libraries was done using the KAPA SYBR® FAST Universal qPCR Kit and an Applied Biosystems 7900HT Real-Time PCR system. Sequencing (100 bp single-end reads) was done on a NovaSeq6000 with standard workflow.

RNA-Seq data processing

Data quality assessment & trimming was done with FastQC & Trimmomatic (Bolger *et al.*, 2014). HISAT2 was used for mapping (TAIR10 genome assembly and the Araport11 annotation were used (Cheng *et al.*, 2017)). Read counting was done with htseq-count. Differential expression analysis was performed with DESeq2 (Love *et al.*, 2014). Differentially Expressed Genes (DEGs) were extracted with $|\log_2$ fold change$| > 1$ and $p_{adj} < 0.05$. Gene Ontology (GO) enrichment analysis and Gene Set Enrichment Analysis (GSEA) were performed using ClusterProfiler *v4.12.6* (Wu *et al.*, 2021). TDT Hub (Transcription Factor-Binding Site Discovery Tool Hub; http://acrab.cnb.csic.es/TDTHub/) was used to predict transcription factor binding site (TFBS) enrichment in promoters of DEGs (Grau et Franco-Zorrilla, 2022). The promoter region, defined as the 3 kb sequence upstream of the translation initiation codon, was analyzed to identify TFBS using the general-purpose tool FIMO (Find Individual Motif occurrences), with a minimum s-score threshold set at 1%.

ICP-OES

Roots and shoots of seedlings were rinsed with Milli-Q water (10 min, 4°C), desorbed by washing twice with 20 mM $CaCl_2$ (10 min, 4°C), once with 10 mM ethylenediaminetetraacetic (EDTA) (10 min, 4°C, pH 5.7) and rinsed one more time with Millipore water (10 min, 4°C). Samples were dried, weighed into PTFE reaction tubes and digested in a microwave oven (START 1500, MLS, Leutkirchen) using a 2:1 mixture of HNO_3 (65%, v/v) and H_2O_2 (30%, v/v). Element concentrations were measured with an iCAP 6500 Series ICP-OES (Thermo-Fisher Scientific).

Thiol profiling with HPLC

For HPLC analysis of thiols, seedlings were grown for 9 d on control plates, transferred to control/Cd plates and harvested after 3 d. Measurements of phytochelatins with HPLC and glutathione were done as described in Pischke *et al.*, (2022).

Results

Cadmium inhibits primary root growth and reduces root apical meristem size

To assess the effect of Cd on primary root growth, *A. thaliana* seedlings were grown for 7 d on control medium and then transferred to either Cd-containing medium or control medium. Primary root elongation was significantly reduced after 24 h and 48 h upon 25 µM Cd exposure, corresponding to a concentration inducing a 50% root growth inhibition after one week (**Figure 1A**). Cadmium exposure also affected the RAM size. A reduction in RAM size was observed after 48 h of Cd treatment, whereas a decrease in the elongation zone (EZ) was evident as early as 24 h of treatment (**Figure 1B-C**). This reduction in RAM size was primarily attributed to a decrease in the number of cortex cells rather than a reduction in cortex cell length, as cell length remained unaffected after 48 h of Cd exposure (**Figure 1D-E**).

Cadmium alters mineral profiles in root parts

As Cd exposure is known to interfere with plant nutrient homeostasis (Haider *et al*., 2021, Hanikenne *et al*., 2021), we analyzed Cd accumulation and its impact on mineral profiles of the root tip (RT, ~2 mm from the apex) and the remaining root (RR) at 24 h and 48 h post-Cd exposure. We first assessed differences in the mineral concentrations between the RT and the RR in control conditions. Cu and P concentrations were significantly higher in RT compared to RR. In contrast, Mn and Zn concentrations were lower in RT compared to RR (**Figure 2A**).

After exposure, Cd accumulation increased over time in both RR and RT. However, Cd concentrations in RT consistently remained lower than in RR, with RT accumulating only 45-47% of the Cd levels found in RR both at 24 h and 48 h (**Figure 2B**). Cadmium treatment influenced mineral partitions between RT and RR. For instance, concentrations of Cu and P decreased at 24 h in RT but were not affected at 48 h (**Figure 2C**). Mn concentrations were reduced after 48 h of Cd treatment in RR. Zn concentrations decreased in all Cd-treated samples compared to controls, except in RT at 48 h (**Figure 2C**). In contrast, minerals with no specific partitioning between RT and RR, like Ni, Mg, and B, were not significantly affected by Cd treatment (**Figure 2C**).

ICP-MS measurements revealed no significant differences in Fe concentrations between Cd-treated and control samples (**Figure 2C**). However, due to Cd's known interference with Fe homeostasis (Lešková et al., 2017) and the presence of outliers in the Fe data, we conducted additional measurements on whole roots using ICP-OES, which revealed a reduction in Fe concentrations upon Cd exposure in Col-0 (**Figure S1**).

Cadmium induces changes in phytochelatins, flavonoids, and glucosinolates content across root parts

To investigate metabolic changes upon Cd exposure in the two root parts, untargeted metabolomic analysis with LC-MS was conducted, detecting a total of 2961 features. Principal Component Analysis (PCA) revealed that the difference between RR and RT overshadowed the variance in metabolic profiles elicited by the treatment with Cd (**Figure 3A**). Importantly, this global trend remained consistent regardless of the normalization method applied, whether based on the number of collected root pieces or the total sum of detected metabolites in each sample(**Figures 3A and S2A**).

The statistical analysis for Differentially Abundant Features (DAFs) revealed 362 features that were less abundant and 369 features that were more abundant after Cd treatment in RR. In RT, 177 DAFs with lower abundance and 372 DAFs with higher abundance due to Cd exposure were identified (**Table S1**).

Among the DAFs, three families were particularly interesting due to their connection with metallic stress response. Indeed, phytochelatin (23 features), flavonoid (49 features), and glucosinolate (23 features) have well-established roles in metal detoxification, stress responses, and antioxidant activity (Lin & Aarts, 2012; Corso *et al.*, 2018; Mitreiter & Gigolashvili, 2020; Shen et al, 2022).

Consistent with their well-known function in metal chelation, phytochelatins increased in both root parts (except one feature in RT), supporting their role in Cd sequestration **(Figures 3B and S2B, Table S1**). Flavonoid accumulation exhibited a root-part-specific pattern, with tricetin, isorhamnetin, and quercetin decreasing in RR, while quercetin and kaempferol increased in RT. Given the antioxidant and metal-binding properties of flavonoids, these differential responses may reflect distinct protective strategies between root compartments (**Figure 3B, Table S1**). Similarly, glucosinolates showed complex and root-part-specific shifts, with differential accumulation of indolic and aliphatic subclasses in RR and RT, potentially influencing redox homeostasis and Cd detoxification mechanisms (**Figure 3B, Table S1**). Additionally, sideretin, the only annotated coumarin, decreased in RR, while no significant change was detected in RT (**Figure S2C**).

Root part is the primary driver of gene expression variance

To assess the effects of Cd on the RR and RT transcriptomes, we performed a transcriptomic analysis after 24 h and 48 h of Cd treatment. Using PCA to evaluate the influence of growth conditions, harvesting time points, and sampled root parts on global gene expression profiles, we identified the root part as the primary factor contributing to transcriptional variance. RT and RR samples were separated along principal component 1 (PC1), which accounted for 95.3% of the observed variance (**Figure 4A**). To understand the biological processes represented by the principal components, we calculated the loading values of each transcript for both components, and identified GO terms enriched among the top and bottom 5% of transcripts with the highest loading values (**Figure S3**). Here, loadings represent the contribution of each transcript to a principal component, with their sign (positive or negative) indicating the direction of the relationship.

GO enrichment analysis of these transcripts for PC1 revealed that this component primarily reflects processes related to specialized metabolite biosynthesis, carbohydrate metabolism, and salt stress responses (**Figures 4A and S3A**). Specifically, transcripts with negative PC1 loadings (indicating higher expression in RR samples) were enriched in specialized metabolite biosynthesis and suberin biosynthetic processes. In contrast, transcripts with positive loadings (indicating higher expression in RT samples) were enriched in carbohydrate metabolism and response to salt stress (**Figure S3A**).

On the other hand, the treatment condition (Cd vs. control) separated samples along principal component 2 (PC2), explaining 2.3% of the variance (**Figure 4A**). GO enrichment analysis of the transcripts contributing most to PC2 showed that positive PC2 loadings (from transcripts more active in Cd-treated samples) were associated with responses to nutrient levels, specialized metabolites, and transition metal ion transport (**Figure S3B**). Conversely, transcripts with negative PC2 loadings (from transcripts more active in control samples) were linked to cellular responses to hypoxia, iron ion regulation, and nutrient-level responses (**Figure S3B**).

Constitutive differences in gene expression between root tips and remaining roots reveal specific functional specialization

Since the root parts accounted for the majority of the observed transcriptional variance, we further explored the constitutive variation in gene expression between RR and RT in control conditions. A total of 4534 genes showed higher expression in RR (up in RR), while 1513 genes exhibited greater expression expressed in RT (up in RT) (**Table S2**). To better understand the constitutive differences between root parts, we performed a GO enrichment analysis. The top GO terms for differentially expressed genes (DEGs) up in RR represented a wide array of processes. Notable terms included those associated with environmental responses (e.g., responses to acid chemicals, water, oxidative stress, and hypoxia) and specialized metabolism (e.g., phenylpropanoid, S-glycoside, and glucosinolate metabolism) (**Figure 4B, Table S3**). In RT, GO terms related to cell wall organization and gravitropism were enriched among the upregulated DEGs, together with a large group of translation-related terms (**Figure 4C, Table S3**).

Given the differences in mineral concentrations between the RT and the RR, together with the enrichment of terms related to nutrition in RR, we examined the relative expression of metal and nutrient transporter genes between root parts. Many were less expressed in RT, including the Fe uptake transporter *IRT1* and the nitrate transporter *NRT2.1*. Conversely, the copper transporter *COPT1* was found to be more expressed in RT compared to RR (**Figure 4D, Table S2**).

Cadmium triggers root part-specific and time-dependent transcriptional responses

We next evaluated the DEGs in response to Cd exposure in contrast to control conditions, in RR and RT, together with the temporal dynamics of this response. In RR, 12 DEGs were unique to 24 h, 51 to 48 h, and 70 were common to both time points. Similarly, in RT, five DEGs were unique to 24 h, 112 to 48 h, and 62 were common to both time points (**Figures 5 and S4, Table S4**). Further, GO enrichment analysis revealed several shared and tissue-specific biological processes affected by Cd exposure.

Shared responses in RR and RT

Both root regions exhibited enrichment in oxidative stress response, response to hypoxia and oxygen levels, and transition metal transport (including iron transport) (**Figure 5A-B, Table S5**). Beyond apparently shared processes, the specific DEGs contributing to the enrichment were not necessarily the same between root parts. For example, *FERRITIN 1* and *4* were downregulated in both RT and RR, contributing to the enrichment of oxidative stress response and metal transport (**Figure S4, Tables S4 and S5)**. In contrast, hydrogen peroxide-responsive genes *HRG1* and *HRG2* were upregulated exclusively in RT (**Figures S4 and S5, Table S4**). Additionally, although not identified in the GO enrichment analysis, *ELIP1* and *ELIP2,* which encode early light-induced proteins (ELIPs) belonging to the multigenic family of pigment-binding light-harvesting complexes with known roles in abiotic stress, were significantly upregulated in both RR and RT, with stronger induction observed in RT under Cd exposure (**Figures S4 and S5, Table S4**).

RR-specific responses

In RR, the top GO terms with the lowest adjusted p-values were enriched at both time points, and were primarily related to stress responses. In addition to the common terms shared with RT, these included responses to nutrient levels (including starvation), extracellular stimulus, ion homeostasis (including manganese (Mn)), and phenylpropanoid metabolism (**Figure 5A, Table S5**).

Transcriptomic changes related to Fe homeostasis in RR were particularly notable, including the specific upregulation of *BASIC HELIX-LOOP-HELIX 38, 39 and 100; IRONMAN 1, 3, 4, 5 and 7; FERRIC REDUCTION OXIDASE 3 and 5* (which also contributed to the enrichment of terms such as response to nutrient levels, extracellular stimulus, and starvation). The downregulation of *VACUOLAR IRON TRANSPORTER-LIKE 1, 2 and 5* also stood out, this latter contributing to the enrichment of the Mn ion homeostasis term (**Tables S4 and S5, Figure S4**).

Interestingly, the phenylpropanoid metabolism genes, *S8H* and *CYP82C4*, which are involved in the coumarin biosynthetic pathway and Fe acquisition (Robe *et al.*, 2021a), were downregulated in RR after 48 h of Cd exposure (**Table S4, Figure S4**). This downregulation aligns with the decrease in sideretin, which was observed in RR upon Cd treatment (**Figure S2C**).

Although sulfur metabolism GO terms were not enriched in Cd-treated RR samples, several DEGs involved in sulfur homeostasis were identified in RR but not in RT, including *RESPONSE TO LOW SULFUR 1, 2* and *3.* Interestingly, *SULPHATE TRANSPORTER 1* was upregulated also in RT at 48 h (**Table S4, Figure S4)**.

RT-specific responses

In RT, a dual response was evident, with some terms enriched at both time points (early response, e.g. oxidative stress, metal ion response) and others enriched only at 48 h (late response, e.g. hypoxia, Fe transport). Cd and Zn-related terms, as well as sulfur compound and glutathione metabolisms, were RT-specific (**Figure 5B, Table S5**).

Transcriptomic changes related to sulfur and glutathione metabolism included the upregulation of glutathione transferase genes *GSTU4, GSTU9*, *GSTU12* and *GSTF7*, as well as *MYB51* and *IGMT2*, which can be linked to altered glucosinolate in RT upon Cd exposure (**Figures 3B, 5B and S4, Table S4)**. *MYB12*, coding a TF involved in flavonoid biosynthesis (Mehrtens et al., 2005) was specifically upregulated in RT (**Table S4, Figures S4 and S5)**. Moreover, RT exhibited a unique transcriptional response linked to cell wall organization and biogenesis, a top upregulated GO category in RT already under control conditions (**Figure 4C**). Genes in this category included XYLOGLUCAN ENDOTRANSGLUCOSYLASE/HYDROLASE (XTH) family genes such as *XTH12, XTH13* and *XTH20* (**Figures S4 and S5, Table S4**).

Finally, Cd treatment reduced root growth and the size of the RAM **(Figure 1A-B**). However, cell division was not identified as a significantly enriched GO term in RT**,** and none of 61 cell cycle-related genes (Vandepoele *et al.,* 2002) were differentially expressed under Cd stress (**Figure S6**). The developmental impact of Cd excess was however reflected in the transcriptomic profiling of RT. Cross-referencing DEGs in RT and RR with cell type-specific expression data (Shahan *et al.,* 2022) revealed increased differentiation of several cell layers in RT under Cd stress. Specifically, 20 genes associated with differentiating cells were upregulated (**Figure S7A**, blue; **Table S6**), including six genes linked to trichoblast elongation and differentiation. Genes related to trichoblast differentiation and xylem pole pericycle differentiation were the most affected, as evidenced by the enrichment profiles of these gene sets in Cd-treated vs control samples (**Figure S7B**).

Many Cd-regulated genes are bZIP transcription factor targets

To explore the regulatory mechanisms underlying the transcriptional response to Cd stress, we analysed the enrichment of transcription factor binding sites (TFBS) in the promoters of DEGs identified in RR and RT at 24 h and 48 h using the TFBS Discovery Tool Hub (Grau & Franco-Zorrilla, 2022). In addition to many MYB-binding motifs, this analysis revealed a significant enrichment of bZIP transcription factor-binding motifs across all comparisons, with the exception of RT at 48 h (**Table S7**). Among bZIP transcription factors, two were differentially expressed after Cd treatment: *bZIP63*, which was downregulated in RT at both time points, and *bZIP1*, which was downregulated in RR at 24 h. However, their binding sites were not detected in the TFBS analysis. Another bZIP transcription factor identified by the promoter analysis of DEGs is ELONGATED HYPOCOTYL 5 (HY5), which is involved in light

signaling, stress responses and nutrient homeostasis (Gangappa & Botto, 2016; Mankotia *et al.*, 2024). Recent studies have furthermore highlighted HY5's role in ROS homeostasis within the root meristem (Gong *et al.,* 2021; Li *et al.*, 2024). Although HY5 did not meet the threshold for differential expression in our RNA-Seq dataset, its expression pattern suggested induction after Cd treatment (**Figure S8**). Supporting a role of HY5 in the Cd response, Gene Set Enrichment Analysis demonstrated that a list of 297 high-confidence HY5 target genes (Burko *et al.,* 2020) was consistently enriched in all comparisons of Cd-treated vs control samples (**Figure S9**).

Overall, the consistent presence of bZIP motifs in DEG promoters suggests a potential role for bZIP transcription factors, and more specifically HY5, in regulating the transcriptional response to Cd stress.

HY5 is a key actor in limiting Cd accumulation and promoting tolerance

To functionally validate these findings, we assessed the Cd sensitivity of *A. thaliana* knock-out mutants for *xth26*, *elip1, elip2*, and *myb12*, whose corresponding genes are directly or indirectly regulated by HY5 (Stracke *et al.*, 2010; Hayami *et al.*, 2015; Burko *et al.*, 2020; Bursch *et al.*, 2020). Given HY5's role in ROS homeostasis, akin to HRG1 and HRG2 (Gong *et al.*, 2021; Li *et al.*, 2024), the phenotypes of *hrg1* and *hrg2* mutants were assessed. The *xth20*, *myb12*, and *hrg2* mutants exhibited a slightly but significantly increased sensitivity to Cd, suggesting their roles in Cd tolerance (**Figure 6A**). Similarly, the *xth26* mutant, though not specifically induced by Cd in RT, showed increased Cd susceptibility compared to Col-0, indicating a potential contribution to Cd tolerance. In contrast, *elip1-elip2* and *hrg1* mutants displayed wild type-like growth under Cd treatment (**Figure S10**). While *xth12* and *xth13* mutants could not be analyzed due to unavailable homozygous lines, these genes remain promising candidates for future studies.

We next directly assessed the Cd sensitivity of two *hy5* knock-out mutants, named *hy5_1* and *hy5_215* (Oyama *et al.*, 1997), in transfer experiments and showed an enhanced sensitivity to Cd compared to the WT (**Figures 6A and S11**). When directly sown on control and Cd plates and grown for 9 d, we observed very little difference in primary root length between Col-0 and *hy5_215* under control conditions (**Figure 6B**). However, the increased Cd sensitivity of the mutant was confirmed. Because the abundance of the HY5 protein is highly dependent on illumination (Zhang *et al.*, 2019), we assessed the Cd phenotype of *hy5* mutants when roots were not lit. We found that both in a root-covered system (RCS) and in complete darkness, *hy5* mutants displayed stronger root growth reduction by Cd than Col-0 (**Figure S11**).

Metal concentrations in roots and shoots of the *hy5* mutants after Cd exposure were analyzed with ICP-OES. Both *hy5_215* and *hy5_1* mutants had higher Cd concentrations in

the roots and shoots compared to Col-0 with *hy5_1* also exhibiting increased Fe content in the roots compared to Col-0 (**Figures 6C** and **S1**). Consistent with the increased Cd accumulation, both *hy5* mutants had increased PC contents (PC2, 3, 4) in the roots, more so than in the shoots, compared to wild type seedlings after Cd exposure (**Figures 6D and S12**).

Discussion

This study analyses the differential responses of *A. thaliana* root tips (RT) and remaining roots (RR) to Cd exposure. The phenotypic impact of Cd on the root apical meristem (RAM) and elongation zone (EZ) have previously been addressed (Yuan & Huang, 2016) and we confirmed a reduction in size of both root regions upon 48 h of Cd stress (**Figure 1**). The spatial separation of RT and RR enabled a specific analysis of the impact of metallic stress on the actively growing tissues in the RT. Additionally, our experimental setting also allowed us to compare the two root regions in control conditions, in particular their metal homeostasis.

Reduced root growth is not accompanied by differential expression of cell cycle regulatory genes

One goal of this study was to analyze the specific impact of Cd on cell cycle activity in the RAM. Even though a reduction of primary root growth by Cd was observed after 24 and 48 h (**Figure 1A**), the transcriptomic data demonstrated that this was not accompanied by the differential expression of such genes (**Figure S6**). Interestingly, a similar observation was made in RT of plants exposed to Zn excess (Thiébaut *et al.,* 2024). This suggests that the mechanisms underlying Cd-induced root growth inhibition might not directly involve transcriptional alterations of cell cycle genes. Indeed, many actors of the cell cycle regulatory machinery, such as cyclin-dependent kinases (CDKs) or cyclins, are known to be regulated at the post-translational level by mechanisms like phosphorylation and proteolysis (Inzé & Veylder, 2006). However, previous research on the cell cycle under Cd stress in RT described effects such as a reduction of the mitotic index (the ratio of cells in mitosis and the total cell number) or an altered expression of cell cycle-related genes (reviewed in Huybrechts *et al.*, 2019). Noteworthy, the latter was reported exclusively in the context of prolonged exposure durations (*i.e.* > 5 d). Thus, the transcriptional regulation of the cell cycle may occur only upon persistent Cd stress.

Elemental concentrations in the two root parts are mirrored by transporter gene expression

Another known effect of Cd stress is ionome alteration. Hence, differences in the ionomic profiles between RR and RT were analyzed together with the expression of transporter genes.

Under control conditions, the concentrations of Cu, Zn, and P differed significantly between RR and RT (**Figure 2)**. Consistent with the higher Cu concentration in RT, *COPT1*, a gene involved in copper acquisition (He *et al.*, 2023), showed higher expression in RT compared to RR (**Figure 2A)**. The lower Zn concentration in RT aligns with the lower expression of several *ZIP* genes (**Figure S4**). However, P was an exception, as its concentration was higher in RT (**Figure 2A,** in accordance with Kanno *et al.*, 2016) despite the lack of correlation with transporter gene expression (**Table S2**). This accumulation likely reflects its essential role in nucleic acids, ATP, and phospholipid composition, as well as its involvement in cell cycle regulation through phosphorylation (Sanchez-Calderon *et al.,* 2005; Ward et al., 2008;Marrocco et al 2010; Veneklaas *et al*., 2012; Genschik et al 2014; Müller *et al*., 2015; Abel, 2017; Li *et al.*, 2017). Additionally, P deficiency severely disrupts RAM function, causing shrinkage and cell cycle arrest (Sanchez-Calderon *et al.,* 2005; Rai, 2014). Consistent with the importance of Pi concentrations in the RAM, the complete root system contributes to the translocation of Pi to this zone, as shown by the rapid translocation of ^{33}P from the root system to the RAM (Kanno et al., 2016). Moreover, the RT plays a key role in Pi uptake and sensing, with high expression of *PHT1;1* and *PHT1;4* in the root cap (Kanno *et al.*, 2016). However, our analysis did not detect this higher transcriptional activity, possibly due to limited root cap contribution in our samples or the absence of Pi starvation conditions. Nevertheless, these findings highlight the contribution of the entire root system to Pi uptake and accumulation in the RAM under control conditions, without contradicting the importance of the RT in Pi homeostasis.

Following Cd treatment, RT accumulated approximately half the Cd levels of RR (**Figure 2B**). This suggests a delayed impact on gene expression in RT compared to RR as indicated by the differential response at 24 and 48 h (**Figure 5**). *IRT1*, the primary Fe(II) uptake transporter known for its role in Cd uptake in *A. thaliana* roots, was found to exhibit large differences in expression between the two root parts (**Figures 4D and S4, Table S2**), which is in agreement with previous reports on the expression of *IRT1* in different root sections (Vert *et al.*, 2002). Similar to *IRT1*, *NRT2.1,* encoding a nitrate transporter which also contributes to Cd uptake (Guan *et al.*, 2021), was less expressed in RT compared to RR. These differences in expression may at least partially account for the reduced Cd concentrations observed in RT compared to RR. Notably, a similar pattern was observed for Zn, under Zn excess conditions, where RT exhibited lower Zn concentrations along with reduced expression of genes encoding Zn uptake transporters (Thiébaut *et al*., 2024). These parallel findings suggest the presence of protective mechanisms limiting the entry of potentially toxic metals into the root apex or reducing their uptake into this zone. To mitigate toxic effects, metals within the cytosol are managed through chelation (e.g. by PCs, see below), exported to the apoplast, or compartmentalized within suitable cellular locations such as the vacuole (Lin & Aarts, 2012).

However, in the RAM, vacuoles are very small, with their size increasing as cells transition into the EZ (Cui *et al.*, 2019; Kaiser & Scheuring, 2020), this may contribute to the observed differences in metal accumulation between RT and RR.

Cadmium triggers many established Fe deficiency responses but suppresses others

At the transcriptomic level, one prominent consequence of Cd exposure was the activation of transcriptomic changes similar to those observed under Fe deficiency (**Figure 4B, C**). Specifically, the repression of *FERRITIN* (Buckhout *et al.*, 2009; Hantzis *et al.*, 2018; von der Mark *et al.*, 2020) and *VTL* (Gollhofer *et al.*, 2014; Tabata *et al.*, 2022) genes, as well as the induction of *bHLH38/39* (Leskova et al. 2017; Kim *et al.*, 2019; Chen *et al.*, 2021), *IRONMAN* (Grillet *et al.*, 2018) and *FRO* (Riaz & Guerinot, 2021) genes have been previously linked to low Fe availability and were also observed under Cd exposure in this study (**Table S4, Figure S4**). Similar to our ICP-OES data (**Figure S1),** Fe concentrations were previously found to be decreased in *A. thaliana* roots upon Cd exposure, possibly due to a competition for the shared uptake of the two metals by the low specificity of the Fe transporter IRT1 (Vert *et al.*, 2002; Lešková *et al.*, 2017).

The activation of an Fe deficiency response under Cd is expected to counteract the systemic Fe deprivation caused by Cd competition. However, Cd exposure resulted in the downregulation of the *S8H* and *CYP82C4* genes, which are involved in the synthesis of catechol-type coumarins, along with a confirmed reduction of the coumarin sideretin content (**Figure S2C**). Coumarins, Fe-mobilizing metabolites derived from the phenylpropanoid pathway, are typically induced under Fe deficiency. In particular, sideretin strongly accumulates under low Fe and especially at acidic pH conditions, as used in this study (Rajniak *et al.*, 2018; Robe *et al.*, 2021a; Vélez-Bermúdez & Schmidt, 2023). Furthermore, an IRT1-independent pathway for Fe uptake via catechol-type coumarin such as fraxetin, complexed with Fe^{3+}, was proposed (Robe *et al.*, 2021b; Vélez-Bermúdez & Schmidt, 2022). Paradoxically, inducing this Fe deficiency response under Cd exposure to enhance Fe mobilization, could unintentionally promote Cd accumulation, as coumarin derivatives can contribute to metal mobilization and uptake complicating further the known interplay between Cd and Fe homeostasis. The observed decrease in sideretin content could therefore reflect an adaptive response to Cd-induced Fe deficiency or a mechanism limiting Cd solubilization in the root environment. Supporting this idea, the *cyp82c4* KO mutant (Rajniak *et al.*, 2018), defective in sideretin synthesis, displayed wild type-like growth under Cd-exposure (**Figure S2D**). While this phytosiderophore-like mechanism challenges the perception that IRT1 exclusively controls Fe entry into root cells, our data strengthen the speculation on a potential role of coumarins in Cd uptake. Notably, the observed increase in both sideretin concentration

and *CYP82C4* expression in RR upon Zn excess (Thiébaut *et al.,* 2024) further supports the consideration that coumarin-mediated uptake may help in the differentiation between essential and non-essential elements.

HY5 affects Cd tolerance and accumulation

HY5, a transcription factor (TF) belonging to the basic leucine zipper (bZIP) family, is well-known for its role in promoting photomorphogenesis. However it also regulates various processes including circadian rhythm, ROS homeostasis, hormone signaling, and nutrient uptake (Gangappa & Botto, 2016; Mankotia *et al.*, 2024). Although HY5 was historically associated with light-regulated development, recent research has uncovered its role in root-specific processes, mediated by its translocation from shoots to roots and its autonomous expression in roots (Chen et al., 2016). Despite these advances, little is known about the specific partners interacting with HY5 in roots and its target genes. Notably, HY5 has been linked to both transcriptional repression and induction of specific genes (Mankotia *et al.* 2023; Mankotia *et al.*, 2024), suggesting a complex regulatory function.

Our results broaden the functional scope of HY5 by revealing a role in Cd tolerance and accumulation. Two independent lines lacking functional HY5 exhibited greater root growth inhibition by Cd than wild type plants (**Figures 6A and S10B**), accompanied by elevated Cd accumulation in roots (**Figure 6C**). This greater Cd accumulation was further associated with increased phytochelatins (PCs) formation (Figure 6D), indicative of higher cytosolic Cd levels, as PC synthases are activated in response to elevated Cd concentrations (Blum et al., 2010). The *hy5* mutants also exhibited higher GSH levels, which are precursors of PCs and main cellular antioxidant. Although HY5 positively regulates sulfur assimilation by activating *APR1* and *APR2*, encoding key enzymes in this pathway, sulfate assimilation and flux through GSH synthesis were not affected in *hy5* mutants (Lee et al., 2011; Mankotia et al., 2024).

Consistently with a role of HY5 in Cd tolerance, transcriptomic analysis revealed multiple HY5 target genes among DEGs in RT under Cd stress, which are associated with cell wall remodeling and redox/ROS homeostasis (Harari-Steinberg *et al.*, 2001; Stracke *et al.*, 2010; Bursch *et al.*, 2020; Gong *et al.*, 2021)(**Figures 6A and S5**). Among those, the repression of *XTH12, 13,* and *26* in the absence of functional HY5 (Bursch et al., 2020) suggests a role for HY5 in modulating cell wall remodeling under stress.

Moreover, several observations suggest that HY5 contributes to maintaining meristem integrity and supporting root growth under Cd stress. This includes the RT-specific upregulation of *HRG1* and *2,* which are crucial for removing H_2O_2 from the RAM (Gong et al., 2021) and the significant increase of several flavonoid features in the RT upon Cd exposure (**Figure 3A**). Flavonoid accumulation has been implicated in Cd detoxification (Corso et al., 2018), as *A.*

thaliana flavonoid biosynthesis and transport knockout mutants exhibited higher Cd sensitivity. Flavonoids can scavenge ROS, quenching H_2O_2 and oxygen free radicals (Agati *et al.,* 2025), thereby mitigating metal-induced oxidative stress. Additionally, their ability to bind metals directly may further contribute to reducing oxidative damage. Given that *MYB12* is a known regulator of flavonoid biosynthesis and is directly regulated by HY5 (Stracke et al., 2010), the increased Cd sensitivity of both *myb12* and *hy5* mutants (**Figure 6A**) suggests that HY5 and MYB12 work together to promote the synthesis of specialized metabolites, such as flavonoids, during Cd stress.

In addition to its role in Cd detoxification, HY5 has an important developmental role, including root morphology (Oyama *et al.*, 1997). Such an impact on root morphology could contribute to modulate Cd uptake. Indeed, changes in root architecture, such as increased root hair length and lateral root density in *hy5* mutants, may also enhance Cd absorption. However, the increased sensitivity to Cd across various light conditions remains stable **(Figure S11**) suggesting that while morphological changes might play a role, altered uptake mechanisms are likely the primary driver of increased Cd accumulation. The involvement of HY5 in Fe homeostasis further connects its regulatory functions to Cd responses and Cd accumulation. Under Cd exposure, Fe concentrations decreased in Col-0 roots but remained stable in *hy5* mutants (**Figure S1**), indicating HY5 is critical for regulating Fe uptake under stress. HY5 promotes Fe acquisition by directly activating *IRT1* and *FRO2* while repressing *BTS* and *PYE* (Mankotia et al., 2023). Paradoxically, HY5 also collaborates with PYE to fine-tune downstream genes like *YSL2*, *YSL3*, and *FRD3*, which mediate Fe distribution and chelation (Mankotia et al., 2024). This dual regulation suggests HY5 balances PYE activity under Cd stress, sufficiently low to maintain Fe uptake (via *IRT1/FRO2*) but restrained to avoid excessive Cd influx through shared transporters. Such complex regulation was already highlighted by Lešková *et al.* (2017). In *hy5* mutants, the absence of HY5-mediated repression may destabilize this equilibrium. However, Fe levels remain stable (potentially due to compensatory PYE self-repression) while *IRT1/FRO2* activity persists, enabling Cd entry.

This study uncovers a novel role for HY5 in limiting Cd accumulation and promoting tolerance, emphasizing HY5 as a central regulator in plant responses to environmental stress, beyond its documented functions in nutrient signaling and uptake (Mankotia *et al*., 2024). Together with the differential responses of the root tip and the remaining root system to Cd exposure, these findings emphasize the need to further investigate the interplay between nutrient homeostasis, stress signaling, and root-specific HY5 activity to better understand plant resilience mechanisms.

Acknowledgements

We thank L. Karim and Dr. W. Coppieters (ULiège, Belgium) for performing the RNA sequencing, Dr. M. Corso (Institut Jean-Pierre Bourgin, France) for support in metabolomics data analyses and Sarah Plößner for assisting in the HPLC measurements. We thank Alok Ranjan for contributing to preliminary experiments. We equally thank Prof. L. Veylder (UGent, Belgium) and Prof. A. Cuypers (UHasselt, Belgium) for helpful discussions at the start of the project. We thank Bert De Rybel (Ghent University, Belgium) and Andras Viczian (University of Szeged, Hungary) for providing the seeds of *myb12-1-f* and *hy5_215*, respectively. Funding was provided by the "Fonds de la Recherche Scientifique-FNRS" (PDR-T0120.18, PDR-T.0104.22 to M.H. and N.V.), the COST ACTION 19116 PLANTMETALS, and the University of Bayreuth (to SC). The IJPB benefits from the support of Saclay Plant Sciences-SPS (ANR-17-EUR-0007). This work has benefited from the support of IJPB's Plant Observatory platform PO-Chem.

Competing interests

The authors declare no competing interests.

Author contributions

NV, SC, NT, LR and MH designed the research. LR, NT, AR and SB performed experiments. LR, NT, SP, SB and MS analyzed the data. LR, NT, SP and MS made the figures. LR, SC, SP, NV, MH, NT and MS wrote the manuscript. All authors read and approved the manuscript.

Data availability

The RNA-Seq reads have been deposited in the National Center for Biotechnology Information (NCBI) Sequence Read Archive (SRA) Database with BioProject identification number PRJNA1208245. The metabolomic data and metadata have been deposited at the MassiVE data repository portal with the identifier MSV000095842. The other data that support the findings of this study are available from the corresponding authors upon reasonable request.

Figure legends

Figure 1. Impact of 25 µM Cd on root growth in *A. thaliana*. A. Primary root growth inhibition by Cd. Seven-day-old seedlings were transferred to control or to 25 µM Cd plates. The progression of growth

was monitored after 24 h, 48 h and one week. Letters indicate statistical significance (ANOVA with Tukey test, $p \leq 0.05$, n=46-76, data from three independent biological replicates, values are mean +/- SD). **B**. RAM size. RAM size was defined as the distance from the quiescent center to the first elongated cortex cell. **C.** EZ size. EZ size was determined by measuring the distance from the first elongated cortex cell to the first root hair. **D.** Number of cortex cells in the RAM. Measurements originate from 10 seedlings per condition and time point (n=10) and one replication. Letters indicate statistically different groups (ANOVA with Tukey test, $p \leq 0.05$**)**. **E.** Cortex cell length. Cortex cell length was determined by dividing the length of RAM by the number of cortex cells in each meristem.

Figure 2. Impact of 25 µM Cd on elemental concentrations in *A. thaliana*. A. Comparison of elemental concentrations in root tips (RT) versus remaining roots (RR) in control conditions. Asterisks indicate statistical significance (Mann-Whitney U-test, $p \leq 0.05$, data from control 24 h and control 48 h were pooled and averaged, n=6). **B.** Cadmium concentrations in RT and RR after exposure**. C.** Elemental concentrations in RT and RR after Cd exposure. Letters indicate statistical significance (ANOVA with Tukey test, $p \leq 0.05$, n=3, data from three independent biological replicates).

Figure 3. Metabolomic analysis of *A. thaliana* root tips (RT) and remaining roots (RR) 48 h after exposure to 25 µM Cd. **A.** Principal component analysis showing the distribution of samples according to PC1 and PC2. The percentage of variance explained by each PC is indicated. Metabolite data were normalized to the total metabolite count in each sample. **B.** Volcano plots showing the metabolic changes in RR and RT after Cd exposure. Significant ($p_{adj} < 0.05$ and $|\log_2 \text{fold change}| > 1$) differentially abundant features (DAFs) are indicated with sky blue, non-significant DAFs are labeled in grey. Features annotated as phytochelatins, flavonoids and glucosinolates are indicated in red.

Figure 4. Differential Expression Analysis between *A. thaliana* root tips (RT) and remaining roots (RR). A. Principal component analysis showing the distribution of samples according to PC1 and PC2. The percentage of variance explained by each PC and enriched GO terms with the highest load in each dimension are indicated in the corresponding axis. **B, C**. GO enrichment analysis for genes with higher expression in RR compared to RT (B) and in RT compared to RR (C) in control conditions. The plots show the top GO terms with the lowest adjusted p-values (FDR), ordered by Gene Ratio (ratio of input genes that are annotated in a term). Circle size corresponds to fold enrichment. **D**. Expression of a selection of genes acting in nutrient uptake in RT vs. RR. Displayed are mean values of $\log_2$ transformed fold changes ± standard deviation.

Figure 5. Differential Expression Analysis in *A. thaliana* root tips (RT) and remaining roots (RR) after exposure to 25 µM Cd for 24 h or 48 h. GO Enrichment of DEGs in RR (**A**) and RT (**B**) at 24 h and 48 h: Shared and Time-Point-Specific Terms. GO enrichment plot showing the top terms with lowest p-adjusted values (FDR) and order by Gene Ratio (ratio of input genes that are annotated in a term). Circles size varies according to the Fold Enrichment. Terms enriched at both time points are presented in color (pink and light blue) and terms present at only one time point are presented in grey. Venn diagrams depict the number of DEGs after 24 h of treatment (light grey), after 48 h of treatment (dark grey), as well as the overlap between the two conditions (pink and light blue).

Figure 6: Phenotypic analysis of cadmium responsive root tip genes in *A. thaliana*. A. Primary root growth of mutants corresponding to candidate genes in the Cd response. Seedlings were grown for 7 days on control plates and then transferred to control/Cd plates for 7 days. Asterisks indicate statistical significance ($p \leq 0.05$, Mann-Whitney U-test, data from three independent replicates, n=15-30). **B**. Representative pictures of Col-0 and *hy5_215* seedlings grown for 9 days directly on either control or Cd plates. **C.** Cd accumulation in Col-0 and *hy5_215* after 3 days of treatment. Displayed are mean values +/- standard deviation of Cd contents as µg per gram dry weight (DW). Letters indicate statistical significance (ANOVA with Tukey test, $p \leq 0.05$, data from three independent replicates) **D.** Phytochelatin (PC) and glutathione (GSH) contents in Col-0 and *hy5_215*. Seedlings were grown for 9 days on control plates and then exposed to Cd or control conditions for 3 days. Displayed are mean values +/- standard deviations of contents in µg per gram fresh weight (FW). Letters indicate statistical significance (ANOVA with Tukey test, $p \leq 0.05$, data from three independent replicates).

References

Abel S. 2017. Phosphate scouting by root tips. Current Opinion in Plant Biology 39: 168–177.

Agati G, Brunetti C, Dos Santos Nascimento LB, Gori A, Lo Piccolo E, Tattini M. **2025**. Antioxidants by nature: an ancient feature at the heart of flavonoids' multifunctionality. *New Phytologist* **245**: 11–26.

Bahmani R, Kim D, Modareszadeh M, Hwang S. **2022**. Cadmium enhances root hair elongation through reactive oxygen species in Arabidopsis. *Environmental and Experimental Botany* **196**: 104813.

Blum R, Meyer KC, Wünschmann J, Lendzian KJ, Grill E. **2010**. Cytosolic Action of Phytochelatin Synthase. *Plant Physiology* **153**: 159–169.

Bolger AM, Lohse M, Usadel B. **2014**. Trimmomatic: a flexible trimmer for Illumina sequence data. *Bioinformatics (Oxford, England)* **30**: 2114–2120.

Boutet S, Barreda L, Perreau F, Totozafy J-C, Mauve C, Gakière B, Delannoy E, Martin-Magniette M-L, Monti A, Lepiniec L, *et al.* 2022. Untargeted metabolomic analyses reveal the diversity and plasticity of the specialized metabolome in seeds of different Camelina sativa genotypes. *The Plant Journal: For Cell and Molecular Biology* **110**: 147–165.

Bruno L, Pacenza M, Forgione I, Lamerton LR, Greco M, Chiappetta A, Bitonti MB. **2017**. In Arabidopsis thaliana Cadmium Impact on the Growth of Primary Root by Altering SCR Expression and Auxin-Cytokinin Cross-Talk. *Frontiers in Plant Science* **8**.

Bucher M. **2007**. Functional biology of plant phosphate uptake at root and mycorrhiza interfaces. *New Phytologist* **173**: 11–26.

Buckhout TJ, Yang TJ, Schmidt W. **2009**. Early iron-deficiency-induced transcriptional changes in Arabidopsis roots as revealed by microarray analyses. *BMC Genomics* **10**: 147.

Burko Y, Seluzicki A, Zander M, Pedmale UV, Ecker JR, Chory J. **2020**. Chimeric Activators and Repressors Define HY5 Activity and Reveal a Light-Regulated Feedback Mechanism[OPEN]. *The Plant Cell* **32**: 967–983.

Bursch K, Toledo-Ortiz G, Pireyre M, Lohr M, Braatz C, Johansson H. **2020**. Identification of BBX proteins as rate-limiting cofactors of HY5. *Nature Plants* **6**: 921–928.

Cabrera J, Conesa CM, del Pozo JC. **2022**. May the dark be with roots: a perspective on how root illumination may bias in vitro research on plant–environment interactions. *New Phytologist* **233**: 1988–1997.

Chen X, Yao Q, Gao X, Jiang C, Harberd NP, Fu X. 2016. Shoot-to-Root Mobile Transcription Factor HY5 Coordinates Plant Carbon and Nitrogen Acquisition. Current Biology 26: 640–646.

Chen W, Zhao L, Liu L, Li X, Li Y, Liang G, Wang H, Yu D. **2021**. Iron deficiency-induced transcription factors bHLH38/100/101 negatively modulate flowering time in *Arabidopsis thaliana*. *Plant Science* **308**: 110929.

Cheng C-Y, Krishnakumar V, Chan AP, Thibaud-Nissen F, Schobel S, Town CD. **2017**. Araport11: a complete reannotation of the Arabidopsis thaliana reference genome. *The Plant Journal* **89**: 789–804.

Clemens S, Aarts MGM, Thomine S, Verbruggen N. **2013**. Plant science: the key to preventing slow cadmium poisoning. *Trends in Plant Science* **18**: 92–99.

Connolly EL, Fett JP, Guerinot ML. **2002**. Expression of the IRT1 Metal Transporter Is Controlled by Metals at the Levels of Transcript and Protein Accumulation. *The Plant Cell* **14**: 1347–1357.

Corso M, Schvartzman MS, Guzzo F, Souard F, Malkowski E, Hanikenne M, Verbruggen N. 2018. Contrasting cadmium resistance strategies in two metallicolous populations of Arabidopsis halleri. *New Phytologist* **218**: 283–297.

Cui Y, Cao W, He Y, Zhao Q, Wakazaki M, Zhuang X, Gao J, Zeng Y, Gao C, Ding Y, *et al.* 2019. A whole-cell electron tomography model of vacuole biogenesis in Arabidopsis root cells. *Nature Plants* **5**: 95–105.

Cui W, Wang H, Song J, Cao X, Rogers HJ, Francis D, Jia C, Sun L, Hou M, Yang Y, *et al.* 2017. Cell cycle arrest mediated by Cd-induced DNA damage in Arabidopsis root tips. *Ecotoxicology and Environmental Safety* **145**: 569–574.

Dello Ioio R, Linhares FS, Scacchi E, Casamitjana-Martinez E, Heidstra R, Costantino P, Sabatini S. **2007**. Cytokinins Determine *Arabidopsis* Root-Meristem Size by Controlling Cell Differentiation. *Current Biology* **17**: 678–682.

Fan SK, Fang XZ, Guan MY, Ye YQ, Lin XY, Du ST, Jin CW. **2014**. Exogenous abscisic acid application decreases cadmium accumulation in Arabidopsis plants, which is associated with the inhibition of IRT1-mediated cadmium uptake. *Frontiers in Plant Science* **5**.

Grau J, Franco-Zorrilla JM. **2022**. TDTHub, a web server tool for the analysis of transcription factor binding sites in plants. *The Plant Journal* **111**(4):1203–1215. https://doi.org/10.1111/tpj.15873

Gangappa SN, Botto JF. **2016**. The Multifaceted Roles of HY5 in Plant Growth and Development. *Molecular Plant* **9**: 1353–1365.

Genschik P, Marrocco K, Bach L, Noir S, Criqui M-C. 2014. Selective protein degradation: a rheostat to modulate cell-cycle phase transitions. Journal of Experimental Botany 65: 2603–2615.

Gollhofer J, Timofeev R, Lan P, Schmidt W, Buckhout TJ. **2014**. Vacuolar-Iron-Transporter1-Like Proteins Mediate Iron Homeostasis in Arabidopsis. *PLOS ONE* **9**: e110468.

Gong F, Yao Z, Liu Y, Sun M, Peng X. **2021**. H_2O_2 response gene 1/2 are novel sensors or responders of H2O2 and involve in maintaining embryonic root meristem activity in *Arabidopsis thaliana*. *Plant Science* **310**: 110981.

Grillet L, Lan P, Li W, Mokkapati G, Schmidt W. **2018**. IRON MAN is a ubiquitous family of peptides that control iron transport in plants. *Nature Plants* **4**: 953–963.

Guan M, Chen M, Cao Z. **2021**. NRT2.1, a major contributor to cadmium uptake controlled by high-affinity nitrate transporters. *Ecotoxicology and Environmental Safety* **218**: 112269.

Haider FU, Liqun C, Coulter JA, Cheema SA, Wu J, Zhang R, Wenjun M, Farooq M. **2021**. Cadmium toxicity in plants: Impacts and remediation strategies. *Ecotoxicology and Environmental Safety* **211**: 111887.

Hanikenne, M., Esteves, S.M., Fanara, S. and Rouached, H. (2021) Coordinated homeostasis of essential mineral nutrients: a focus on iron J. Balk, ed. *Journal of Experimental Botany*, **72**, 2136–2153.

Hantzis LJ, Kroh GE, Jahn CE, Cantrell M, Peers G, Pilon M, Ravet K. **2018**. A Program for Iron Economy during Deficiency Targets Specific Fe Proteins. *Plant Physiology* **176**: 596–610.

Harari-Steinberg O, Ohad I, Chamovitz DA. **2001**. Dissection of the Light Signal Transduction Pathways Regulating the Two Early Light-Induced Protein Genes in Arabidopsis. *Plant Physiology* **127**: 986–997.

Hayami N, Sakai Y, Kimura M, Saito T, Tokizawa M, Iuchi S, Kurihara Y, Matsui M, Nomoto M, Tada Y, *et al.* 2015. The Responses of Arabidopsis *Early Light-Induced Protein2* to Ultraviolet B, High Light, and Cold Stress Are Regulated by a Transcriptional Regulatory Unit Composed of Two Elements. *Plant Physiology* **169**: 840–855.

He L, Ma H, Song W, Zhou Z, Ma C, Zhang H. **2023**. Arabidopsis COPT1 copper transporter uses a single histidine to regulate transport activity and protein stability. *International Journal of Biological Macromolecules* **241**: 124404.

Howden R, Goldsbrough PB, Andersen CR, Cobbett CS. **1995**. Cadmium-Sensitive, *cad1* Mutants of *Arabidopsis thaliana* Are Phytochelatin Deficient. *Plant Physiology* **107**: 1059–1066.

Huybrechts M, Cuypers A, Deckers J, Iven V, Vandionant S, Jozefczak M, Hendrix S. **2019**. Cadmium and Plant Development: An Agony from Seed to Seed. *International Journal of Molecular Sciences* **20**: 3971.

Inzé D, Veylder LD. **2006**. Cell Cycle Regulation in Plant Development1. *Annual Review of Genetics* **40**: 77–105.

Ishimaru Y, Takahashi R, Bashir K, Shimo H, Senoura T, Sugimoto K, Ono K, Yano M, Ishikawa S, Arao T, *et al.* 2012. Characterizing the role of rice NRAMP5 in Manganese, Iron and Cadmium Transport. *Scientific Reports* **2**: 286.

Ismael MA, Elyamine AM, Moussa MG, Cai M, Zhao X, Hu C. **2019**. Cadmium in plants: uptake, toxicity, and its interactions with selenium fertilizers. *Metallomics* **11**: 255–277.

Jia Z, Giehl RFH, Hartmann A, Estevez JM, Bennett MJ, Wirén N von. **2023**. A spatially concerted epidermal auxin signaling framework steers the root hair foraging response under low nitrogen. *Current Biology* **33**: 3926-3941.e5.

Kaiser S, Scheuring D. **2020**. To Lead or to Follow: Contribution of the Plant Vacuole to Cell Growth. *Frontiers in Plant Science* **11**.

Kanno S, Arrighi J-F, Chiarenza S, Bayle V, Berthomé R, Péret B, Javot H, Delannoy E, Marin E, Nakanishi TM, *et al.* 2016. A novel role for the root cap in phosphate uptake and homeostasis (D Weigel, Ed.). *eLife* **5**: e14577.

Kim SA, LaCroix IS, Gerber SA, Guerinot ML. **2019**. The iron deficiency response in *Arabidopsis thaliana* requires the phosphorylated transcription factor URI. *Proceedings of the National Academy of Sciences* **116**: 24933–24942.

Kumar S, Kumar S, Mohapatra T. **2021**. Interaction Between Macro- and Micro-Nutrients in Plants. *Frontiers in Plant Science* **12**: 665583.

Lee B, Koprivova A, Kopriva S. 2011. The key enzyme of sulfate assimilation, adenosine 5′-phosphosulfate reductase, is regulated by HY5 in Arabidopsis. The Plant Journal 67: 1042–1054.

Lešková A, Giehl RFH, Hartmann A, Farga¡ová A, von Wirén N. **2017**. Heavy Metals Induce Iron Deficiency Responses at Different Hierarchic and Regulatory Levels. *Plant Physiology* **174**: 1648–1668.

Leonardo B, Emanuela T, Letizia MM, Antonella M, Marco M, Fabrizio A, Beatrice BM, Adriana C. **2021**. Cadmium affects cell niches maintenance in *Arabidopsis thaliana* post-embryonic shoot and root apical meristem by altering the expression of WUS/WOX homolog genes and cytokinin accumulation. *Plant Physiology and Biochemistry* **167**: 785–794.

Li Y, Jin K, Bunker E, Zhang X, Luo X, Liu X, Hao B. **2018**. Structural basis of the phosphorylation-independent recognition of cyclin D1 by the SCF^{FBXO31} ubiquitin ligase. *Proceedings of the National Academy of Sciences* **115**: 319–324.

Li J, Zeng J, Tian Z, Zhao Z. **2024**. Root-specific photoreception directs early root development by HY5-regulated ROS balance. *Proceedings of the National Academy of Sciences* **121**: e2313092121.

Lin Y-F, Aarts MGM. **2012**. The molecular mechanism of zinc and cadmium stress response in plants. *Cellular and Molecular Life Sciences* **69**: 3187–3206.

Love MI, Huber W, Anders S. **2014**. Moderated estimation of fold change and dispersion for RNA-seq data with DESeq2. *Genome Biology* **15**: 550.

Lux A, Martinka M, Vaculík M, White PJ. **2011**. Root responses to cadmium in the rhizosphere: a review. *Journal of Experimental Botany* **62**: 21–37.

Mankotia S, Singh D, Monika K, Kalra M, Meena H, Meena V, Yadav RK, Pandey AK, Satbhai SB. **2023**. ELONGATED HYPOCOTYL 5 regulates *BRUTUS* and affects iron acquisition and homeostasis in *Arabidopsis thaliana*. *The Plant Journal* **114**: 1267–1284.

Mankotia S, Jakhar P, Satbhai SB. **2024**. HY5: a key regulator for light-mediated nutrient uptake and utilization by plants. *New Phytologist* **241**: 1929–1935.

von der Mark C, Ivanov R, Eutebach M, Maurino VG, Bauer P, Brumbarova T. **2020**. Reactive oxygen species coordinate the transcriptional responses to iron availability in Arabidopsis. *Journal of Experimental Botany* **72**: 2181–2195.

Marrocco K, Bergdoll M, Achard P, Criqui M-C, Genschik P. 2010. Selective proteolysis sets the tempo of the cell cycle. Current Opinion in Plant Biology 13: 631–639.

Mase K, Tsukagoshi H. **2021**. Reactive Oxygen Species Link Gene Regulatory Networks During Arabidopsis Root Development. *Frontiers in Plant Science* **12**: 660274.

Mehrtens F, Kranz H, Bednarek P, Weisshaar B. **2005**. The Arabidopsis Transcription Factor MYB12 Is a Flavonol-Specific Regulator of Phenylpropanoid Biosynthesis. *Plant Physiology* **138**: 1083–1096.

Miotto YE, da Costa CT, Offringa R, Kleine-Vehn J, Maraschin F dos S. **2021**. Effects of Light Intensity on Root Development in a D-Root Growth System. *Frontiers in Plant Science* **12**: 778382.

Mitreiter S, Gigolashvili T. **2021**. Regulation of glucosinolate biosynthesis (H Takahashi, Ed.). *Journal of Experimental Botany* **72**: 70–91.

Müller J, Toev T, Heisters M, Teller J, Moore KL, Hause G, Dinesh DC, Bürstenbinder K, Abel S. **2015**. Iron-Dependent Callose Deposition Adjusts Root Meristem Maintenance to Phosphate Availability. *Developmental Cell* **33**: 216–230.

Oyama T, Shimura Y, Okada K. **1997**. The Arabidopsis HY5 gene encodes a bZIP protein that regulates stimulus-induced development of root and hypocotyl. *Genes & Development* **11**: 2983–2995.

Paffrath V, Tandron Moya YA, Weber G, Von Wirén N, Giehl RFH. **2024**. A major role of coumarin-dependent ferric iron reduction in strategy I-type iron acquisition in Arabidopsis. *The Plant Cell* **36**: 642–664.

Perilli S, Di Mambro R, Sabatini S. **2012**. Growth and development of the root apical meristem. *Current Opinion in Plant Biology* **15**: 17–23.

Perilli S, Moubayidin L, Sabatini S. **2010**. The molecular basis of cytokinin function. *Current Opinion in Plant Biology* **13**: 21–26.

Pischke E, Barozzi F, Colina Blanco AE, Kerl CF, Planer-Friedrich B, Clemens S. **2022**. Dimethylmonothioarsenate Is Highly Toxic for Plants and Readily Translocated to Shoots. *Environmental Science & Technology* **56**: 10072–10083.

Rahim HU, Akbar WA, Alatalo JM. **2022**. A Comprehensive Literature Review on Cadmium (Cd) Status in the Soil Environment and Its Immobilization by Biochar-Based Materials. *Agronomy* **12**: 877.

Rai V, Sanagala R, Sinilal B, Yadav S, Sarkar AK, Dantu PK, Jain A. **2015**. Iron Availability Affects Phosphate Deficiency-Mediated Responses, and Evidence of Cross-Talk with Auxin and Zinc in Arabidopsis. *Plant and Cell Physiology* **56**: 1107–1123.

Rajniak J, Giehl RFH, Chang E, Murgia I, von Wirén N, Sattely ES. **2018**. Biosynthesis of redox-active metabolites in response to iron deficiency in plants. *Nature chemical biology* **14**: 442–450.

Ren M, Li Y, Zhu J, Zhao K, Wu Z, Mao C. **2023**. Phenotypes and Molecular Mechanisms Underlying the Root Response to Phosphate Deprivation in Plants. *International Journal of Molecular Sciences* **24**: 5107.

Riaz N, Guerinot ML. **2021**. All together now: regulation of the iron deficiency response. *Journal of Experimental Botany* **72**: 2045–2055.

Robe K, Conejero G, Gao F, Lefebvre-Legendre L, Sylvestre-Gonon E, Rofidal V, Hem S, Rouhier N, Barberon M, Hecker A, *et al.* 2021a. Coumarin accumulation and trafficking in *Arabidopsis thaliana*: a complex and dynamic process. *New Phytologist* **229**: 2062–2079.

Robe K, Stassen M, Chamieh J, Gonzalez P, Hem S, Santoni V, Dubos C, Izquierdo E. **2021b**. Uptake of Fe-fraxetin complexes, an IRT1 independent strategy for iron acquisition in *Arabidopsis thaliana*. *Biorxiv.* doi.org/10.1101/2021.08.03.454955.

Růžička K, Šimášková M, Duclercq J, Petrášek J, Zažímalová E, Simon S, Friml J, Van Montagu MCE, Benková E. **2009**. Cytokinin regulates root meristem activity via modulation of the polar auxin transport. *Proceedings of the National Academy of Sciences* **106**: 4284–4289.

Sánchez-Calderón L, López-Bucio J, Chacón-López A, Cruz-Ramírez A, Nieto-Jacobo F, Dubrovsky JG, Herrera-Estrella L. 2005. Phosphate Starvation Induces a Determinate Developmental Program in the Roots of Arabidopsis thaliana. Plant and Cell Physiology 46: 174–184.

Shahan R, Hsu CW, Nolan TM, Cole BJ, Taylor IW, Greenstreet L, Zhang S, Afanassiev A, Vlot AHC, Schiebinger G, et al. 2022. A single-cell Arabidopsis root atlas reveals developmental trajectories in wild-type and cell identity mutants. Developmental Cell **57**: 543-560.e9.

Shen N, Wang T, Gan Q, Liu S, Wang L, Jin B. **2022**. Plant flavonoids: Classification, distribution, biosynthesis, and antioxidant activity. *Food Chemistry* **383**: 132531.

Spielmann J, Ahmadi H, Scheepers M, Weber M, Nitsche S, Carnol M, Bosman B, Kroymann J, Motte P, Clemens S, *et al.* 2020. The two copies of the zinc and cadmium ZIP6 transporter of *Arabidopsis halleri* have distinct effects on cadmium tolerance. *Plant, Cell & Environment* **43**: 2143–2157.

Stracke R, Favory J-J, Gruber H, BarTELniewoehner L, BarTELs S, Binkert M, Funk M, Weisshaar B, Ulm R. **2010**. The Arabidopsis bZIP transcription factor HY5 regulates expression of the PFG1/MYB12 gene in response to light and ultraviolet-B radiation. *Plant, Cell & Environment* **33**: 88–103.

Tabata R, Kamiya T, Imoto S, Tamura H, Ikuta K, Tabata M, Hirayama T, Tsukagoshi H, Tanoi K, Suzuki T, *et al.* 2022. Systemic Regulation of Iron Acquisition by Arabidopsis in Environments with Heterogeneous Iron Distributions. *Plant and Cell Physiology* **63**: 842–854.

Tao L, Zhu H, Luo X, Li J, Ru Y, Lv J, Pan W, Li Y, Li X, Chen Y, *et al.* 2024. Manganese toxicity elicits the degradation of auxin transport carriers to restrain arabidopsis root growth. *Environmental and Experimental Botany* **225**: 105863.

Thiébaut N, Richtmann L, Sarthou M, Persson DP, Ranjan A, Schloesser M, Boutet S, Rezende L, Assunção A, Clemens S, Verbruggen N, Hanikenne M. Specific redox and iron homeostasis responses in the root tip of Arabidopsis upon zinc excess. *Biorxiv.* doi.org/10.1101/2024.08.29.610234 (Accepted with minor revision in *New Phytologist).*

Tsukagoshi H, Busch W, Benfey PN. **2010**. Transcriptional Regulation of ROS Controls Transition from Proliferation to Differentiation in the Root. *Cell* **143**: 606–616.

Vandepoele K, Raes J, De Veylder L, Rouzé P, Rombauts S, Inzé D. **2002**. Genome-Wide Analysis of Core Cell Cycle Genes in Arabidopsis. *The Plant Cell* **14**: 903–916.

Vélez-Bermúdez IC, Schmidt W. **2022**. How Plants Recalibrate Cellular Iron Homeostasis. *Plant and Cell Physiology* **63**: 154–162.

Vélez-Bermúdez IC, Schmidt W. **2023**. Plant strategies to mine iron from alkaline substrates. *Plant and Soil* **483**: 1–25.

Veneklaas EJ, Lambers H, Bragg J, Finnegan PM, Lovelock CE, Plaxton WC, Price CA, Scheible W, Shane MW, White PJ, et al. 2012. Opportunities for improving phosphorus-use efficiency in crop plants. New Phytologist 195: 306–320.

Vert G, Grotz N, Dédaldéchamp F, Gaymard F, Guerinot ML, Briat J-F, Curie C. **2002**. IRT1, an Arabidopsis Transporter Essential for Iron Uptake from the Soil and for Plant Growth. *The Plant Cell* **14**: 1223–1233.

Wang R, Fei Y, Pan Y, Zhou P, Adegoke JO, Shen R, Lan P. **2023**. IMA peptides function in iron homeostasis and cadmium resistance. *Plant Science: An International Journal of Experimental Plant Biology* **336**: 111868.

Wang H-Q, Xuan W, Huang X-Y, Mao C, Zhao F-J. **2021**. Cadmium Inhibits Lateral Root Emergence in Rice by Disrupting OsPIN-Mediated Auxin Distribution and the Protective Effect of OsHMA3. *Plant and Cell Physiology* **62**: 166–177.

Ward JT, Lahner B, Yakubova E, Salt DE, Raghothama KG. **2008**. The Effect of Iron on the Primary Root Elongation of Arabidopsis during Phosphate Deficiency. *Plant Physiology* **147**: 1181–1191.

Wells DM, Wilson MH, Bennett MJ. **2010**. Feeling UPBEAT about Growth: Linking ROS Gradients and Cell Proliferation. *Developmental Cell* **19**: 644–646.

Wu H, Chen C, Du J, Liu H, Cui Y, Zhang Y, He Y, Wang Y, Chu C, Feng Z, *et al.* 2012. Co-Overexpression FIT with AtbHLH38 or AtbHLH39 in Arabidopsis-Enhanced Cadmium Tolerance via Increased Cadmium Sequestration in Roots and Improved Iron Homeostasis of Shoots. *Plant Physiology* **158**: 790–800.

Wu T, Hu E, Xu S, Chen M, Guo P, Dai Z, Feng T, Zhou L, Tang W, Zhan L, *et al.* 2021. clusterProfiler 4.0: A universal enrichment tool for interpreting omics data. *The Innovation* **2**: 100141.

Yang S-Y, Lin W-Y, Hsiao Y-M, Chiou T-J. **2024**. Milestones in understanding transport, sensing, and signaling of the plant nutrient phosphorus. *The Plant Cell* **36**: 1504–1523.

Yuan H-M, Huang X. **2016**. Inhibition of root meristem growth by cadmium involves nitric oxide-mediated repression of auxin accumulation and signalling in Arabidopsis. *Plant, Cell & Environment* **39**: 120–135.

Zhai Z, Gayomba SR, Jung H, Vimalakumari NK, Piñeros M, Craft E, Rutzke MA, Danku J, Lahner B, Punshon T, *et al.* 2014. OPT3 Is a Phloem-Specific Iron Transporter That Is Essential for Systemic Iron Signaling and Redistribution of Iron and Cadmium in Arabidopsis. *The Plant Cell* **26**: 2249–2264.

Zhang Y, Wang C, Xu H, Shi X, Zhen W, Hu Z, Huang J, Zheng Y, Huang P, Zhang K-X, *et al.* 2019. HY5 Contributes to Light-Regulated Root System Architecture Under a Root-Covered Culture System. *Frontiers in Plant Science* **10**.

Zhou M, Zhang LL, Ye JY, Zhu QY, Du WX, Zhu YX, Liu XX, Lin XY, Jin CW. **2021**. Knockout of *FER* decreases cadmium concentration in roots of *Arabidopsis thaliana* by inhibiting the pathway related to iron uptake. *Science of The Total Environment* **798**: 149285.

Supporting Information

Supplementary Figure S1. ICP-OES measurement of Cd (left) and Fe (right) in Col-0 and *hy5_1* seedlings upon exposure to 25 µM Cd.

Supplementary Figure S2. Regulation of specialized metabolism in response to 25 µM Cd.

Supplementary Figure S3. GO enrichment analysis on the 5% top and bottom loading values for PC1 and PC2.

Supplementary Figure S4. Expression of metal-related genes after 24 h and 48 h of Cd treatment in *A. thaliana* roots.

Supplementary Figure S5. Gene Expression and phenotypic analysis of root tip responsive genes in *A. thaliana*.

Supplementary Figure S6. Effect of 25 µM Cd on expression of cell cycle-related genes from Vandepoele *et al.*, (2002) in root tips (RT) after 24 h and 48 h

Supplementary Figure S7. Impact of Cd excess on differentiation in *A. thaliana* roots.

Supplementary Figure S8: Expression pattern of *HY5*.

Supplementary Figure S9: Gene Set Enrichment Analysis of HY5 targets genes.

Supplementary Figure S10: Phenotypic analysis of root tip-responsive gene mutants under Cd stress.

Supplementary Figure S11: Primary root growth of *hy5_1* and *hy5_215* under exposure to 25 µM Cd in a root covered system and in darkness.

Supplementary Figure S12: Phytochelatin (PC) and glutathione contents in Col-0 and *hy5_1* upon exposure to 25 µM Cd.

Supplementary Table S1: DAFs in RR and RT after 48 h of Cd exposure.

Supplementary Table S2: DEGs in RR vs RT under control conditions.

Supplementary Table S3: Complete list of GO enriched terms in DEGs in RR vs RT.

Supplementary Table S4: DEGs in RR and RT after 24 h or 48 h of Cd exposure.

Supplementary Table S5: GO enrichment analysis of DEGs at 24 h and 48 h, Cadmium vs Control. Shared and time-point specific terms.

Supplementary Table S6: Impact of Cd excess on differentiation in Arabidopsis roots.

Supplementary Table S7: TFBS enrichment in promoters of DEGs.

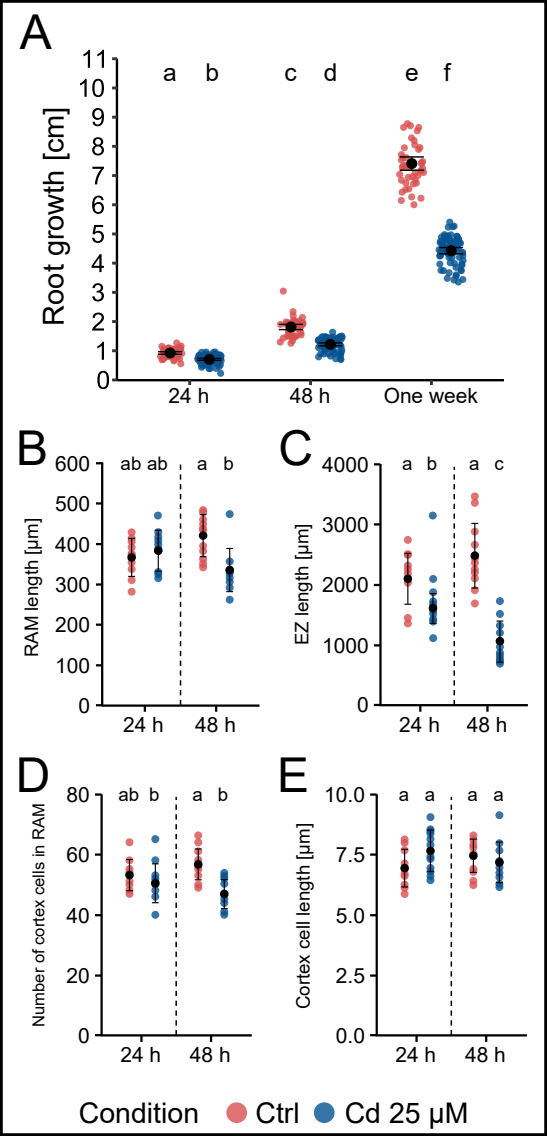
A
Root growth [cm]
a b c d e f
24 h
48 h
One week
B
RAM length [µm]
ab ab a b
C
EZ length [µm]
a b a c
D
Number of cortex cells in RAM
ab b a b
E
Cortex cell length [µm]
a a a a
Condition
Ctrl
Cd 25 µM

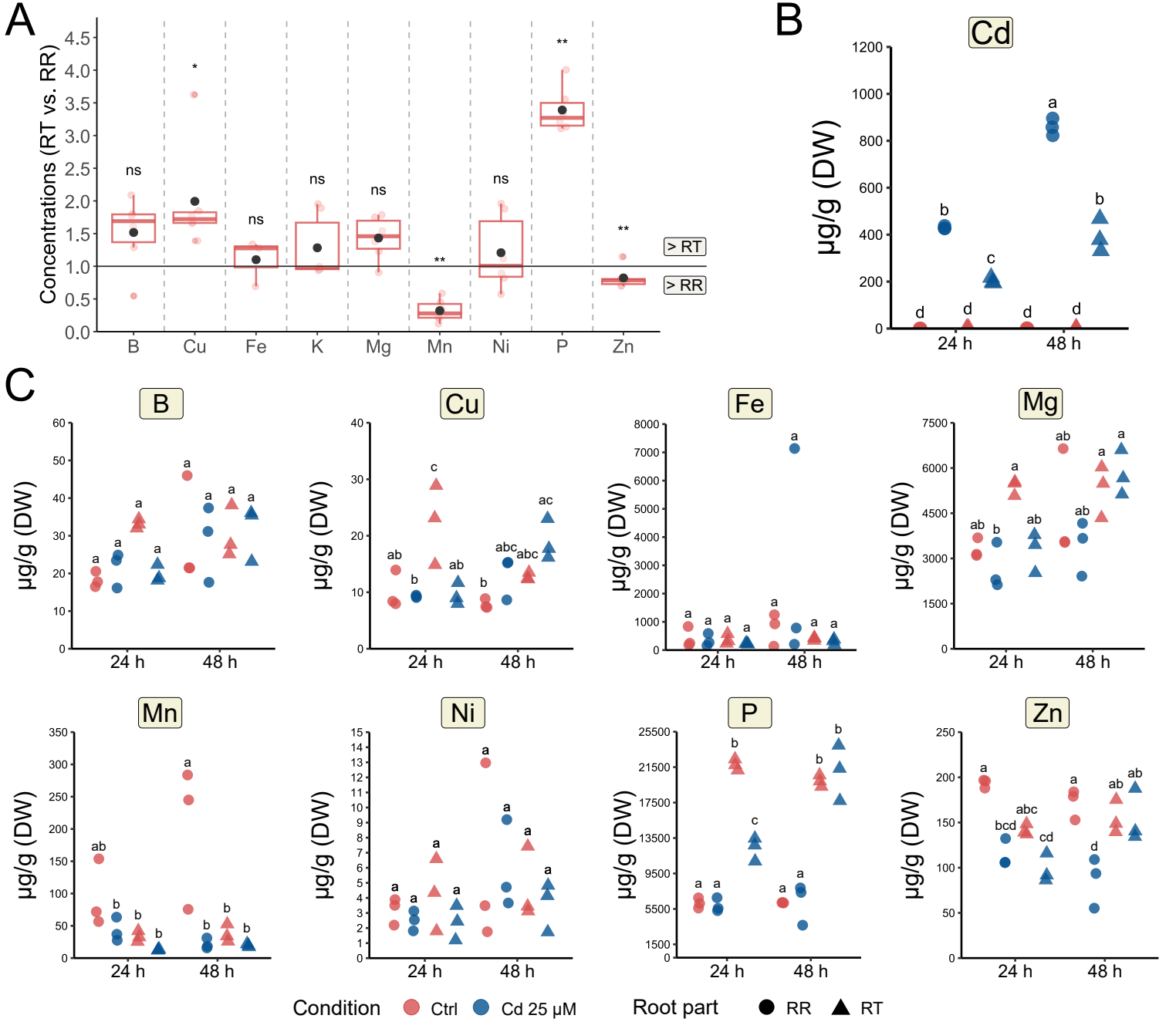
A
Concentrations (RT vs. RR)
B
Cu
Fe
K
Mg
Mn
Ni
P
Zn
ns
*
**
> RT
> RR
B
Cd
µg/g (DW)
24 h
48 h
C
Fe
Mg
Mn
Ni
Zn
Condition
Ctrl
Cd 25 µM
Root part
RR
RT

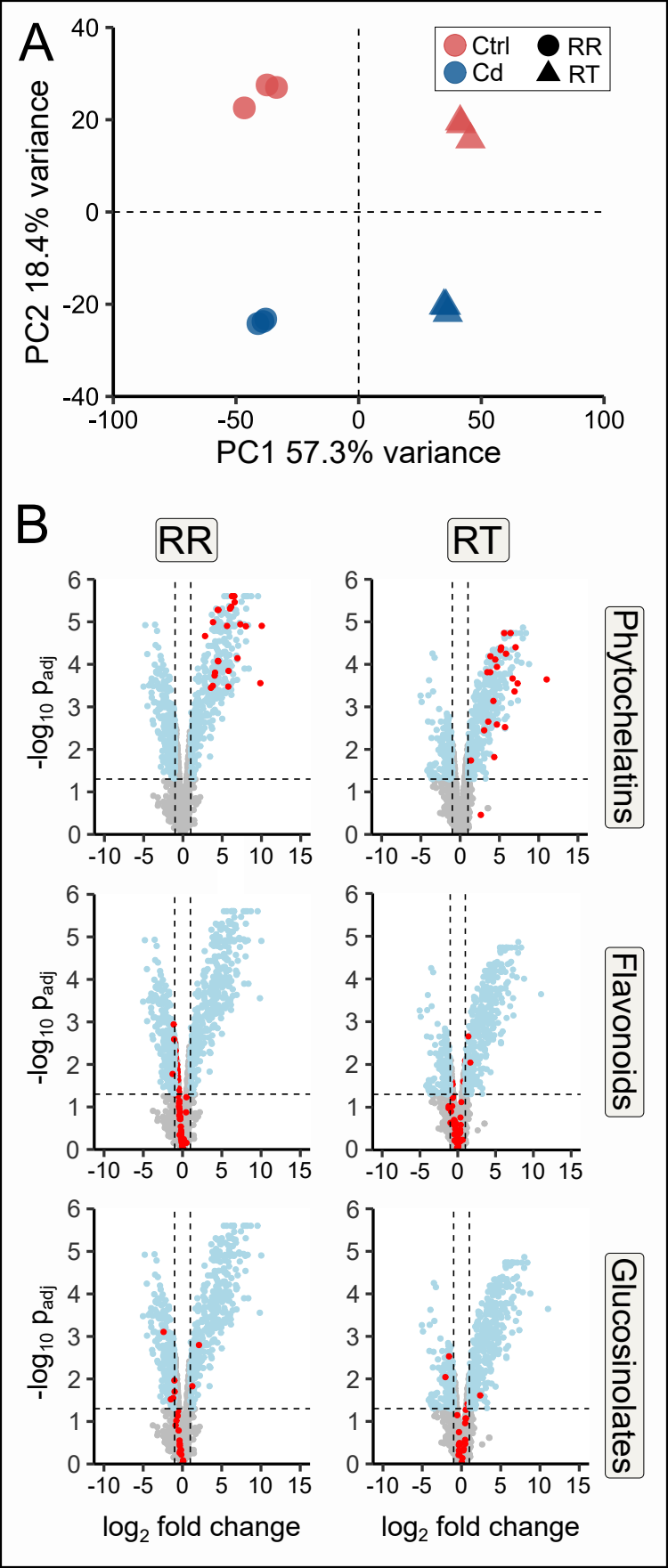
A
Ctrl
Cd
RR
RT
PC2 18.4% variance
PC1 57.3% variance
B
RR
RT
Phytochelatins
Flavonoids
Glucosinolates
-log10 padj
log2 fold change

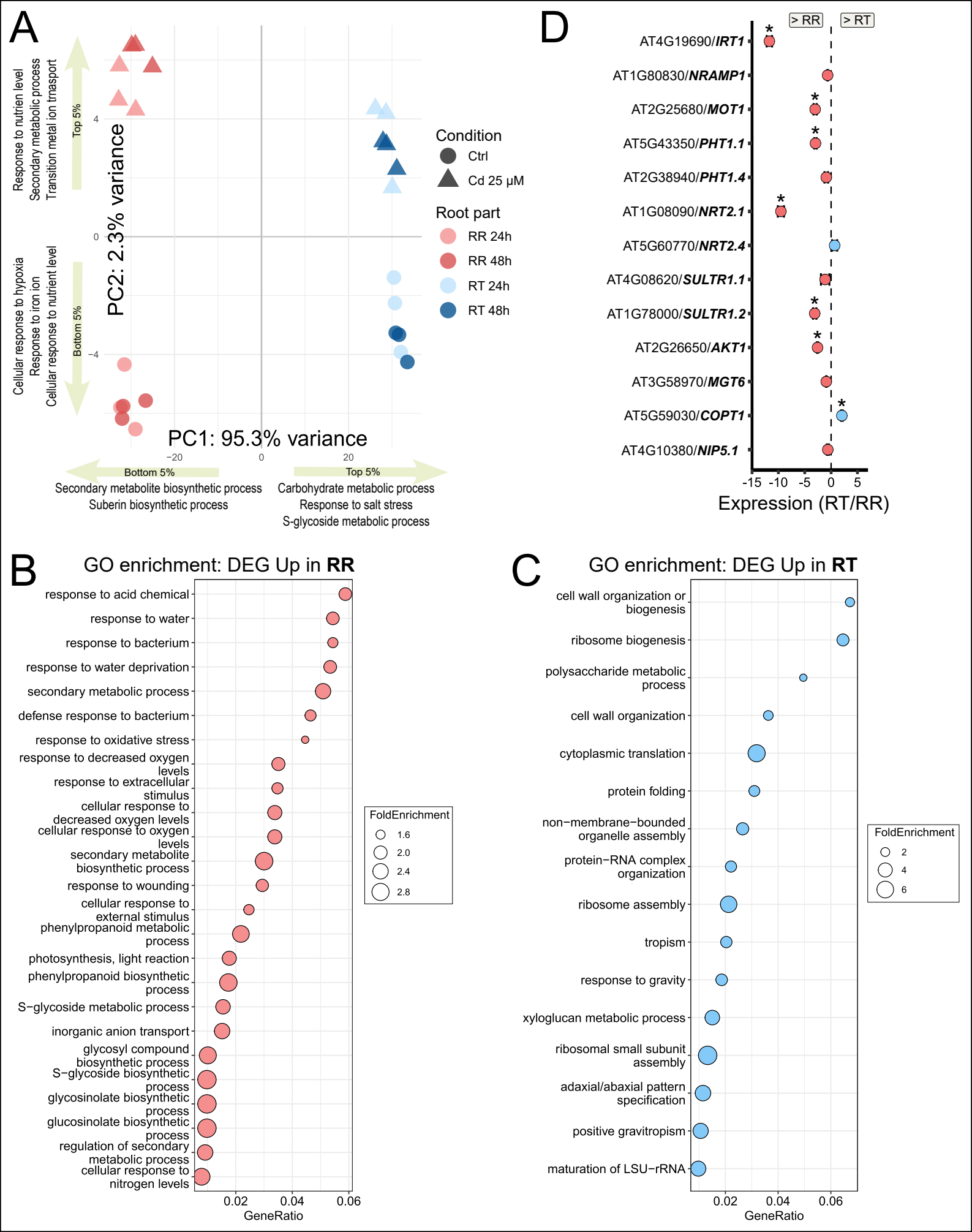
A
Response to nutrien level
Secondary metabolic process
Transition metal ion tmasport
Top 5%
Cellular response to hypoxia
Response to iron ion
Cellular response to nutrient level
Bottom 5%
PC2: 2.3% variance
PC1: 95.3% variance
Bottom 5%
Secondary metabolite biosynthetic process
Suberin biosynthetic process
Top 5%
Carbohydrate metabolic process
Response to salt stress
S-glycoside metabolic process
Condition
Ctrl
Cd 25 µM
Root part
RR 24h
RR 48h
RT 24h
RT 48h
D
> RR
> RT
AT4G19690/IRT1
AT1G80830/NRAMP1
AT2G25680/MOT1
AT5G43350/PHT1.1
AT2G38940/PHT1.4
AT1G08090/NRT2.1
AT5G60770/NRT2.4
AT4G08620/SULTR1.1
AT1G78000/SULTR1.2
AT2G26650/AKT1
AT3G58970/MGT6
AT5G59030/COPT1
AT4G10380/NIP5.1
Expression (RT/RR)
B
GO enrichment: DEG Up in RR
response to acid chemical
response to water
response to bacterium
response to water deprivation
secondary metabolic process
defense response to bacterium
response to oxidative stress
response to decreased oxygen levels
response to extracellular stimulus
cellular response to decreased oxygen levels
cellular response to oxygen levels
secondary metabolite biosynthetic process
response to wounding
cellular response to external stimulus
phenylpropanoid metabolic process
photosynthesis, light reaction
phenylpropanoid biosynthetic process
S−glycoside metabolic process
inorganic anion transport
glycosyl compound biosynthetic process
S−glycoside biosynthetic process
glycosinolate biosynthetic process
glucosinolate biosynthetic process
regulation of secondary metabolic process
cellular response to nitrogen levels
GeneRatio
FoldEnrichment
C
GO enrichment: DEG Up in RT
cell wall organization or biogenesis
ribosome biogenesis
polysaccharide metabolic process
cell wall organization
cytoplasmic translation
protein folding
non−membrane−bounded organelle assembly
protein−RNA complex organization
ribosome assembly
tropism
response to gravity
xyloglucan metabolic process
ribosomal small subunit assembly
adaxial/abaxial pattern specification
positive gravitropism
maturation of LSU−rRNA
GeneRatio
FoldEnrichment

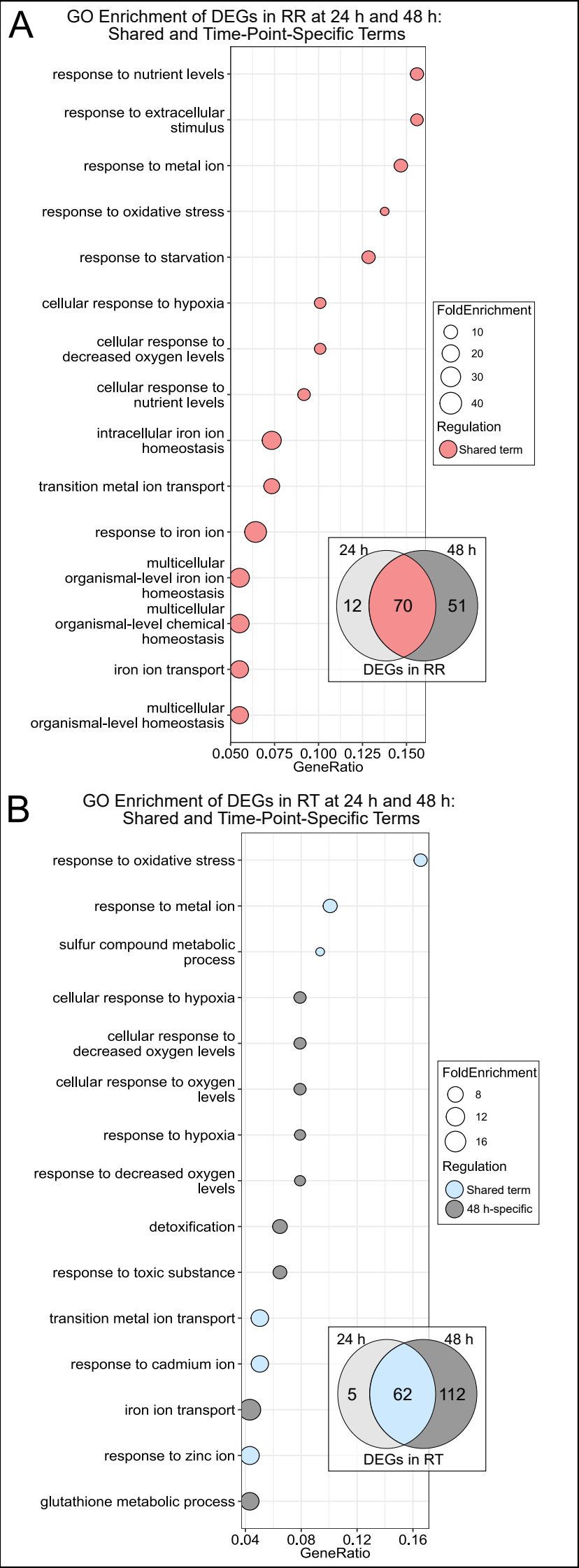
A
GO Enrichment of DEGs in RR at 24 h and 48 h:
Shared and Time-Point-Specific Terms
response to nutrient levels
response to extracellular stimulus
response to metal ion
response to oxidative stress
response to starvation
cellular response to hypoxia
cellular response to decreased oxygen levels
cellular response to nutrient levels
intracellular iron ion homeostasis
transition metal ion transport
response to iron ion
multicellular organismal-level iron ion homeostasis
multicellular organismal-level chemical homeostasis
iron ion transport
multicellular organismal-level homeostasis
0.050 0.075 0.100 0.125 0.150
GeneRatio
FoldEnrichment
10
20
30
40
Regulation
Shared term
24 h
48 h
12
70
51
DEGs in RR
B
GO Enrichment of DEGs in RT at 24 h and 48 h:
Shared and Time-Point-Specific Terms
response to oxidative stress
response to metal ion
sulfur compound metabolic process
cellular response to hypoxia
cellular response to decreased oxygen levels
cellular response to oxygen levels
response to hypoxia
response to decreased oxygen levels
detoxification
response to toxic substance
transition metal ion transport
response to cadmium ion
iron ion transport
response to zinc ion
glutathione metabolic process
0.04 0.08 0.12 0.16
GeneRatio
FoldEnrichment
8
12
16
Regulation
Shared term
48 h-specific
24 h
48 h
5
62
112
DEGs in RT

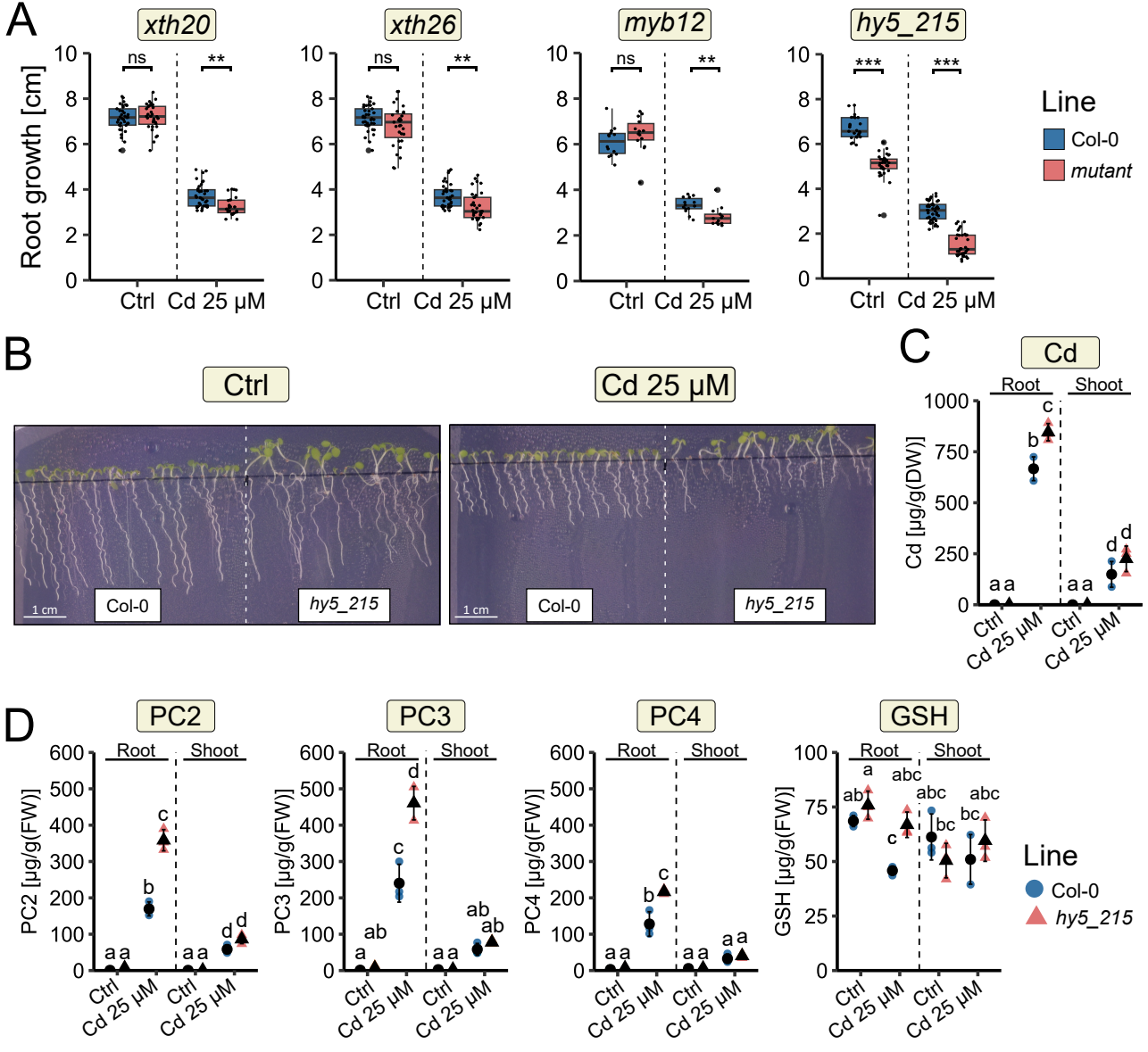
A
xth20
xth26
myb12
hy5_215
Root growth [cm]
ns
**
***
Ctrl
Cd 25 µM
Line
Col-0
mutant
B
Ctrl
Cd 25 µM
1 cm
Col-0
hy5_215
C
Cd
Root
Shoot
Cd [µg/g(DW)]
D
PC2
PC3
PC4
GSH
PC2 [µg/g(FW)]
PC3 [µg/g(FW)]
PC4 [µg/g(FW)]
GSH [µg/g(FW)]
Line
Col-0
hy5_215

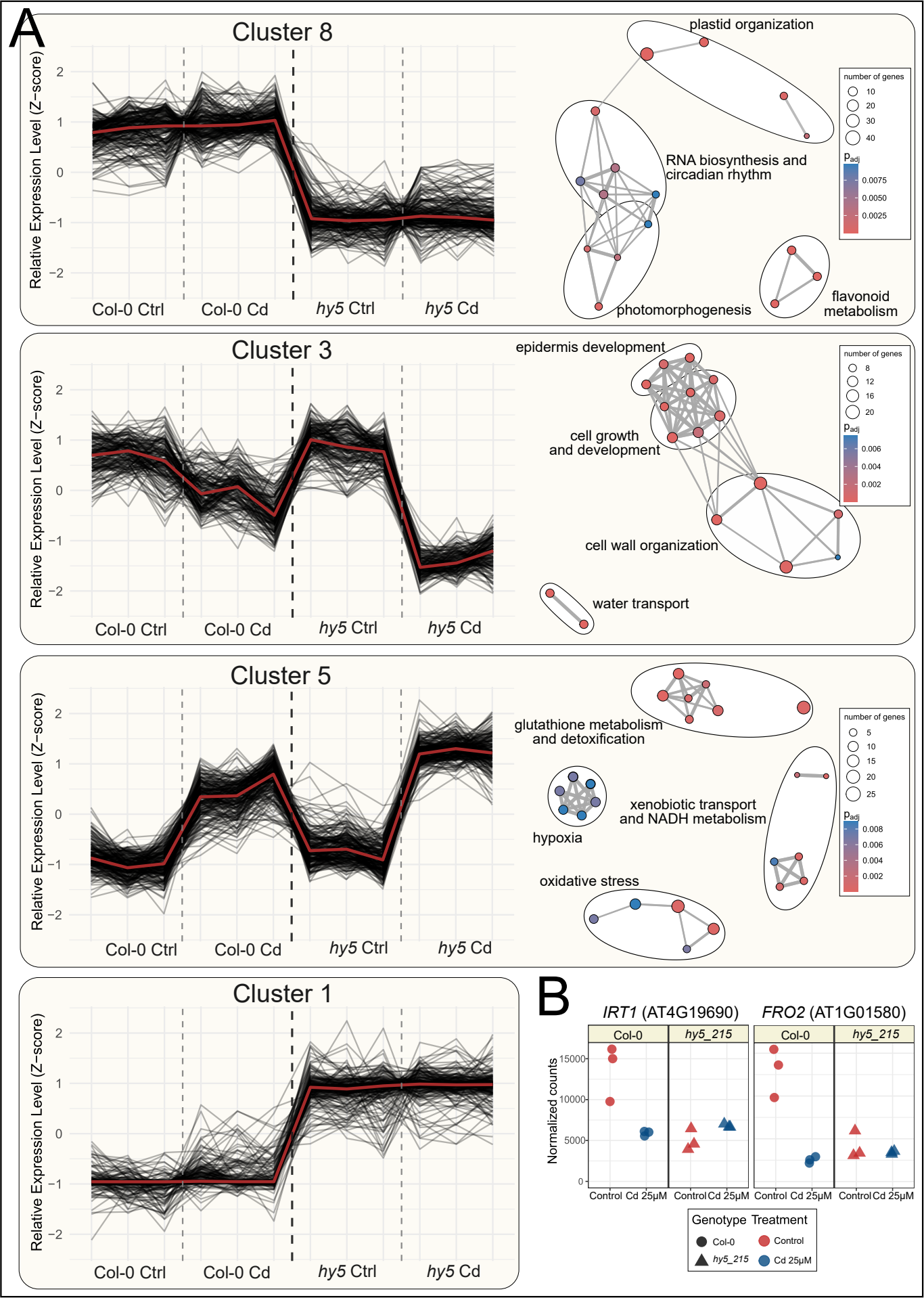
A
Cluster 8
Relative Expression Level (Z−score)
Col-0 Ctrl
Col-0 Cd
hy5 Ctrl
hy5 Cd
plastid organization
RNA biosynthesis and circadian rhythm
photomorphogenesis
flavonoid metabolism
number of genes
10
20
30
40
padj
0.0075
0.0050
0.0025
Cluster 3
epidermis development
cell growth and development
cell wall organization
water transport
number of genes
8
12
16
20
padj
0.006
0.004
0.002
Cluster 5
glutathione metabolism and detoxification
hypoxia
xenobiotic transport and NADH metabolism
oxidative stress
number of genes
5
10
15
20
25
padj
0.008
0.006
0.004
0.002
Cluster 1
B
IRT1 (AT4G19690)
FRO2 (AT1G01580)
Col-0
hy5_215
Normalized counts
Control
Cd 25μM
Genotype
Treatment
Col-0
hy5_215
Control
Cd 25μM

Arabidopsis thaliana root responses to Cd exposure: insights into root tip-specific changes and the role of HY5 in limiting Cd accumulation and promoting tolerance

Ludwig Richtmann, Santiago Prochetto, Noémie Thiébaut, Manon Sarthou, Stéphanie Boutet, Marc Hanikenne, Stephan Clemens and Nathalie Verbruggen.

Supplementary Figures

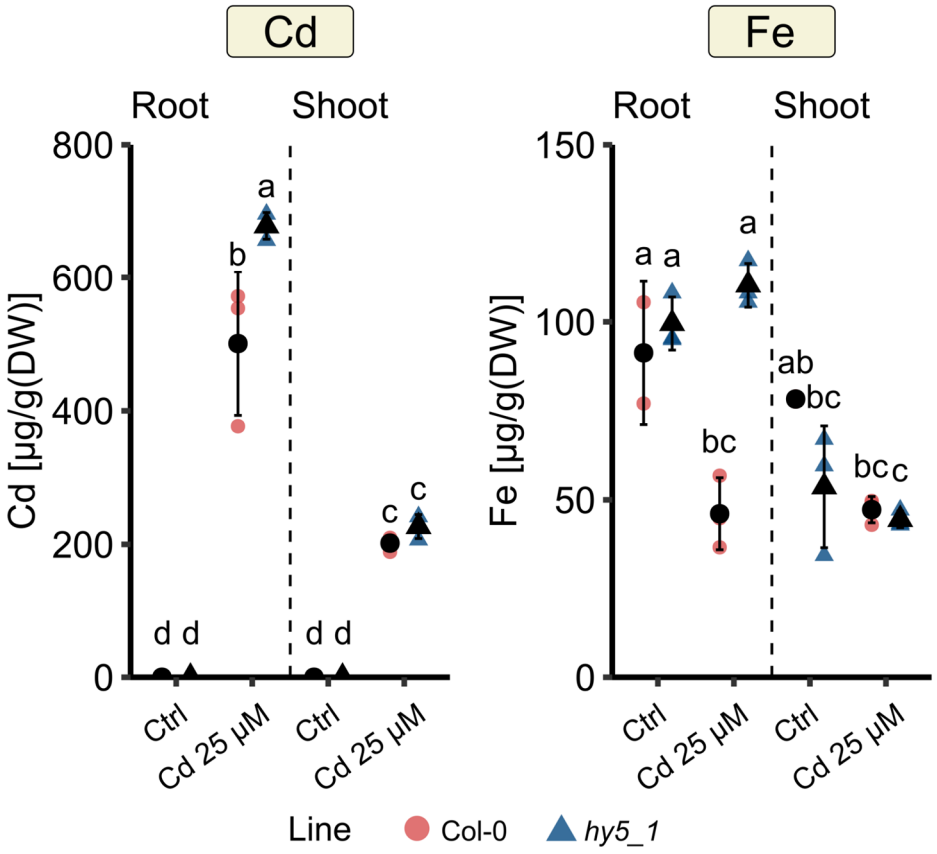

Supplementary Figure S1. ICP-OES measurement of Cd (left) and Fe (right) in Col-0 and *hy5_1* seedlings upon exposure to 25 µM Cd. Seedlings were grown for 7 d on control medium and then transferred to control or Cd medium and exposed for 72 h. Displayed mean values +/- standard deviation of Cd contents as µg per gram dry weight (DW). Letters indicate statistical significance (ANOVA with Tukey test, p≤0.05, data from at least three independent replicates).

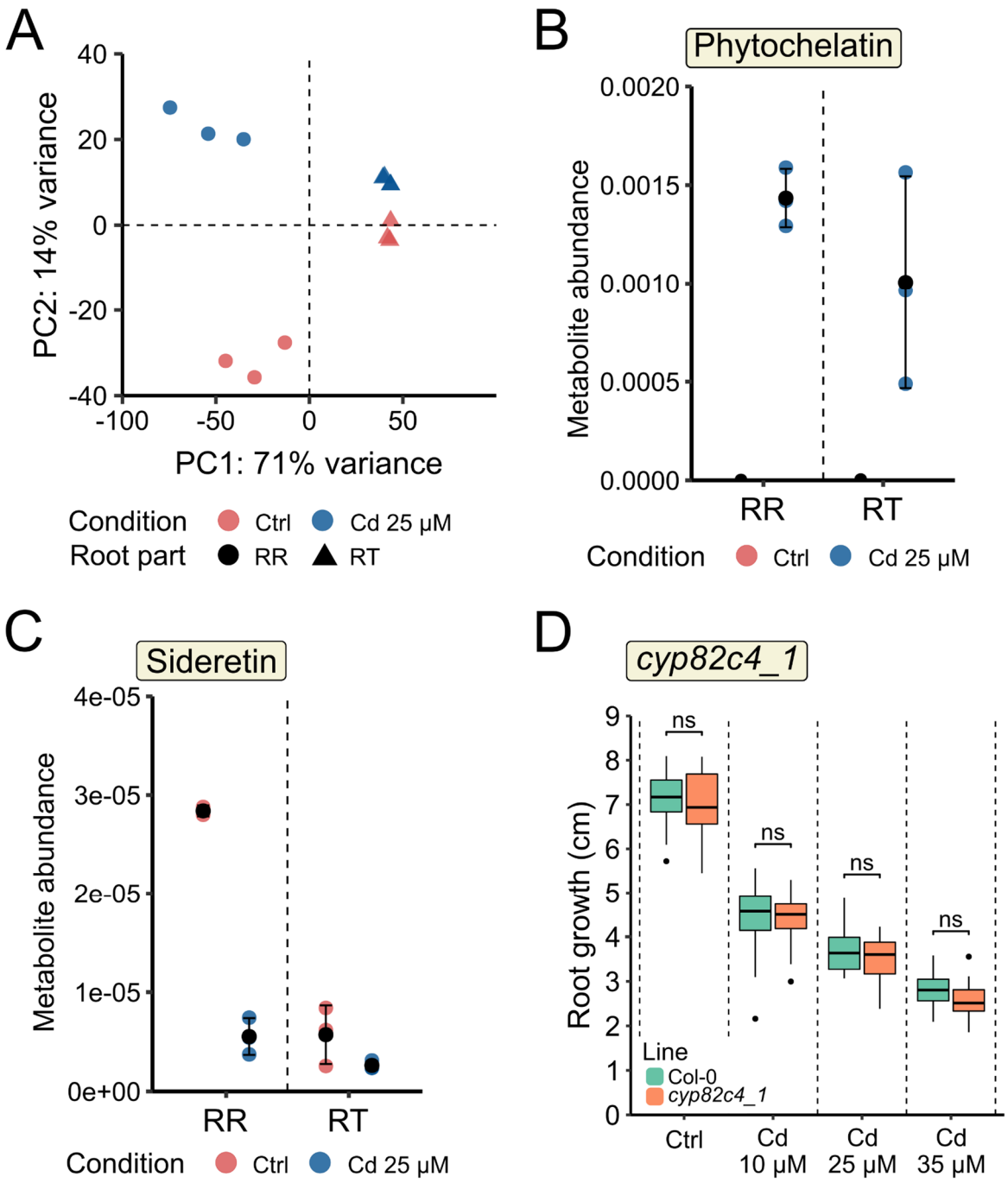

Supplementary Figure S2. Regulation of specialized metabolism in response to 25 µM Cd. A. Principal component analysis of the metabolomic data. Metabolite concentrations were normalized to the amount of collected root pieces per sample. **B**-**C.** Quantification of sideretin and phytochelatin in control and Cd in root tips (RT) and remaining roots (RR). Seedlings were grown for 7 d on control medium and then exposed to 25 µM Cd for 48 h. **D.** Primary root growth of Col-0 and the *cyp82c4* mutant under control and Cd conditions. Statistical significance was tested with Mann Whitney U-Test (n=24-37, 3 independent replicates, p≤0.05)

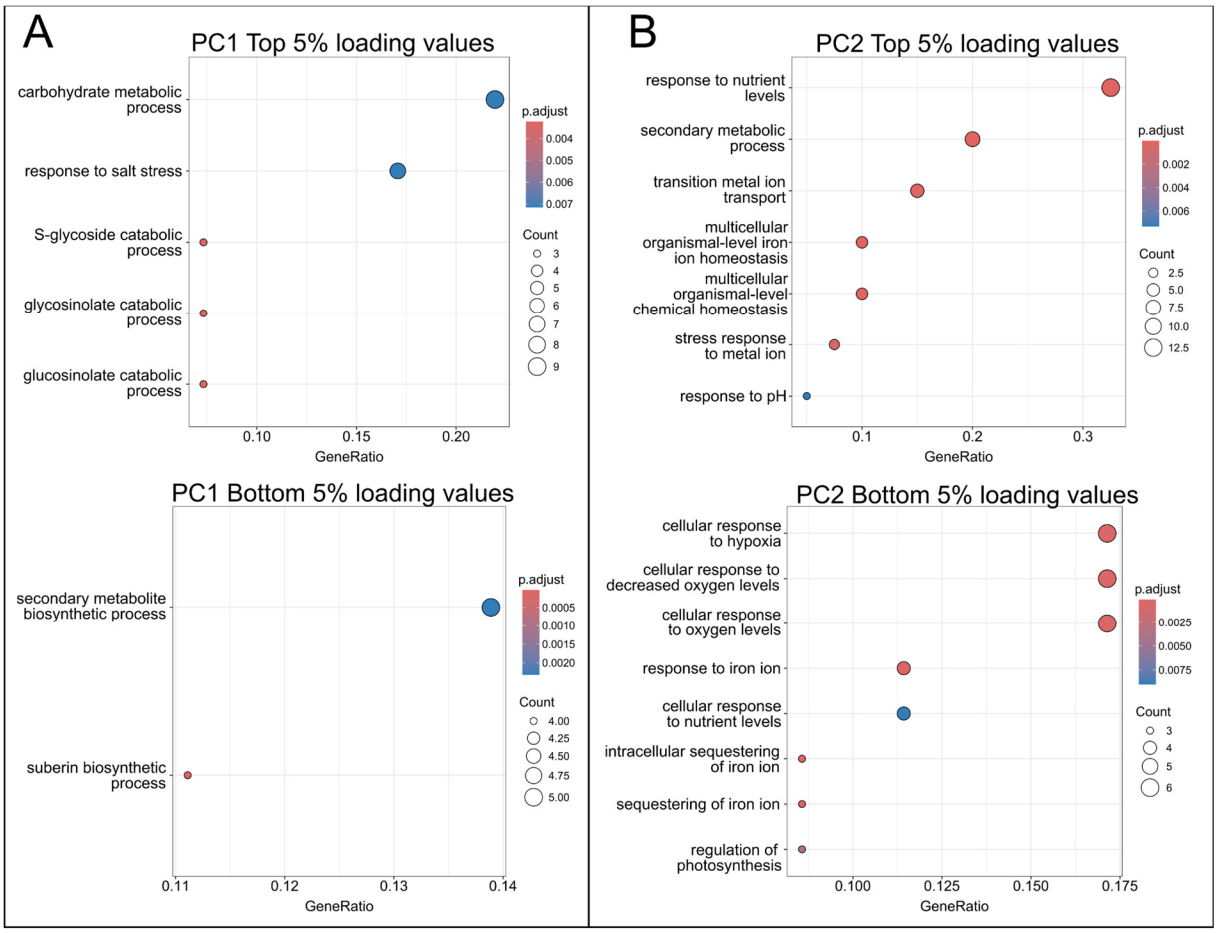

Supplementary Figure S3. GO enrichment analysis on the 5% top and bottom loading values for PC1 (A) and PC2 (B). The analysis was conducted using the ClusterProfiler package in R, which identifies overrepresented GO terms associated with the input gene sets. Enriched GO terms (Biological Process) were selected based on a false discovery rate (FDR) < 0.01. Dot Size represents the number of genes associated with each GO term; dot color, the adjusted p-value (FDR); and GeneRatio the proportion of genes in the input set associated with the GO term.

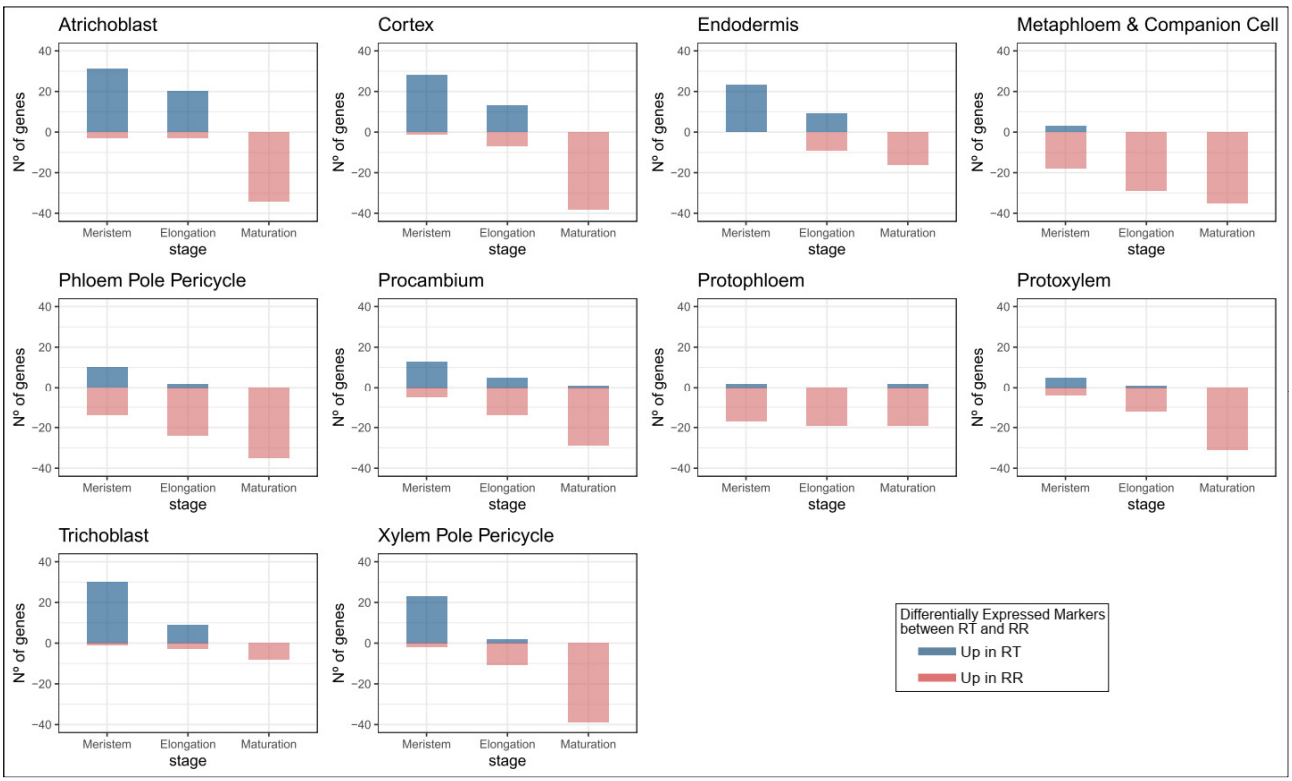

Supplementary Figure S4. Differentially expressed markers between RT and RR. Bulk RNA-Seq data from root tip (RT) and remaining root (RR) samples upon growth in control conditions were cross-referenced with the cell-type specific description of gene expression in roots provided by Shahan *et al.*, (2022). Number of genes differentially expressed ($|\log_2$ fold change$| > 1$ and $p_{adj} \leq 0.05$) between RT and RR samples that are among the 50 genes that are specific markers for each cell line and development stage. Positive and negative values in the Y-axis represent the number of DEGs that are more expressed in RT or RR, respectively.

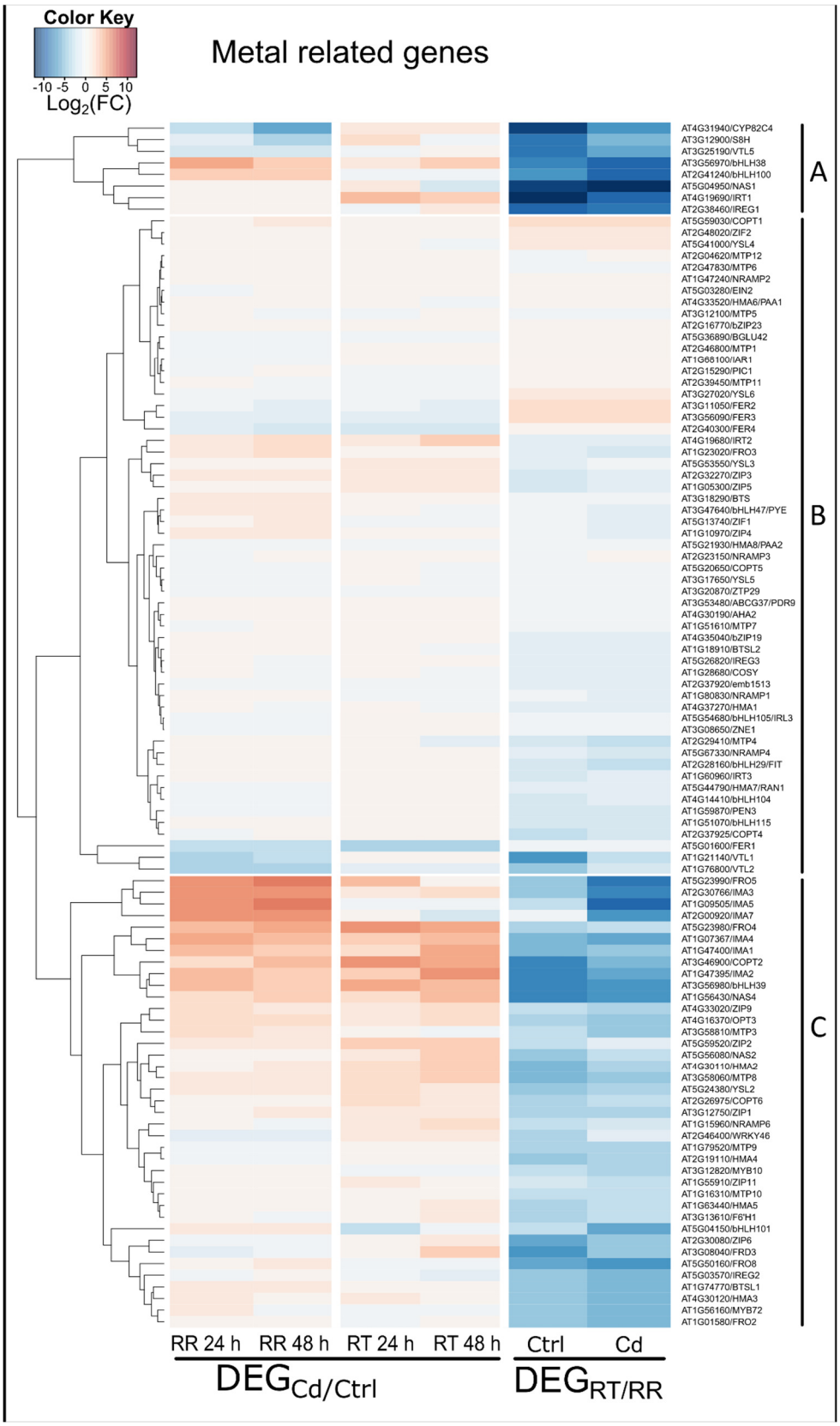

Supplementary Figure S5. Expression of metal-related genes after 24 h and 48 h of Cd treatment in *A. thaliana* roots. Using a manually curated list of metal related genes, the heatmap shows the log2(fold change) of gene expression between conditions. In the $DEG_{Cd/Ctrl}$ columns, positive values indicate upregulation of genes after Cd treatment, while negative values indicate downregulation, in both the remaining root (RR) and root tip (RT) after 24 h or 48 h of treatment. In the $DEG_{RT/RR}$ columns, positive values indicate higher expression in RT compared to RR, while negative values indicate higher expression in RR compared to RT.

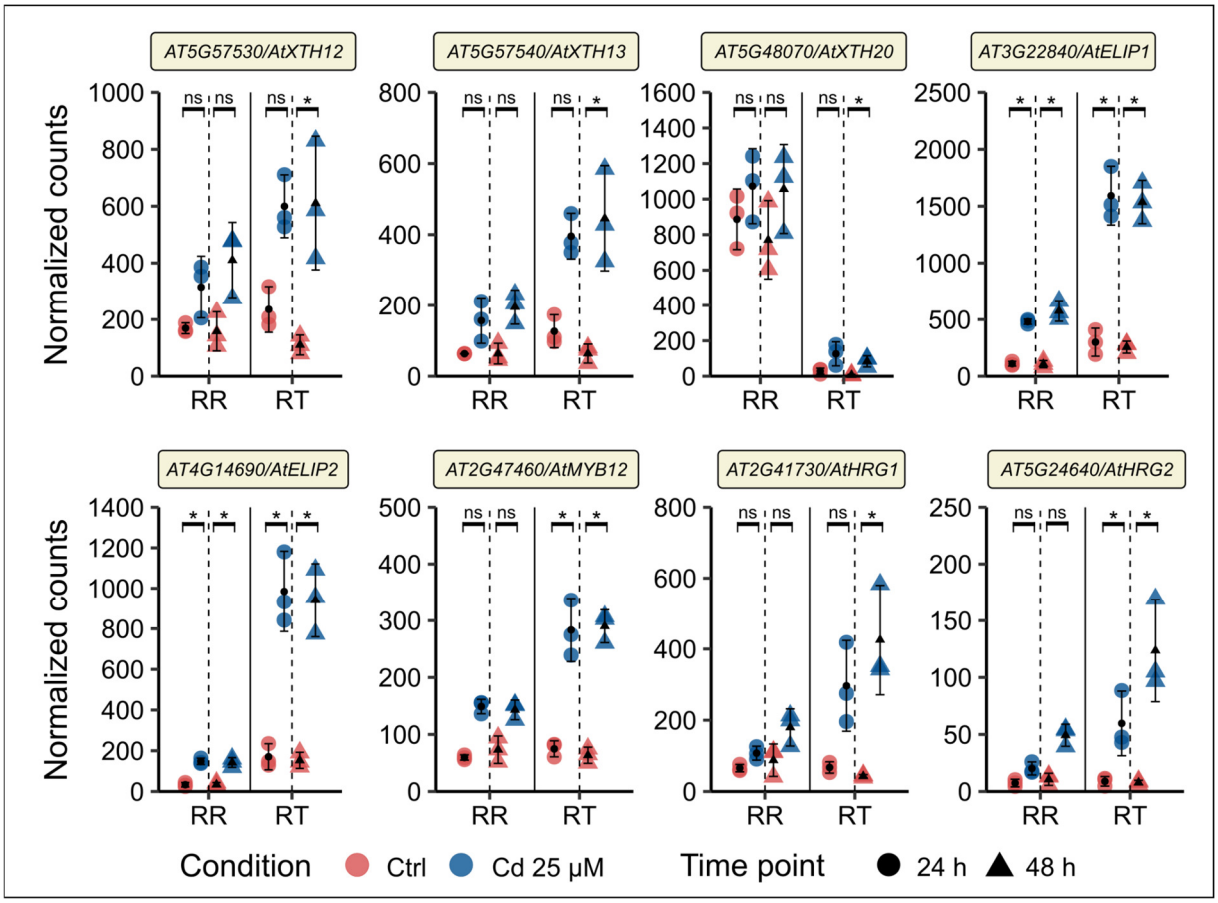

Supplementary Figure S6. Gene expression and phenotypic analysis of root tip responsive genes in *A. thaliana*. A. Expression of genes that display a specific or more pronounced response to Cd in RT compared to RR. Displayed are mean values ± standard deviation. Asterisks indicate statistical significance of DEG (DESeq2, $|\log_2$ fold change$| > 1$ and $p_{adj} \leq 0.05$, data from three independent replicates).

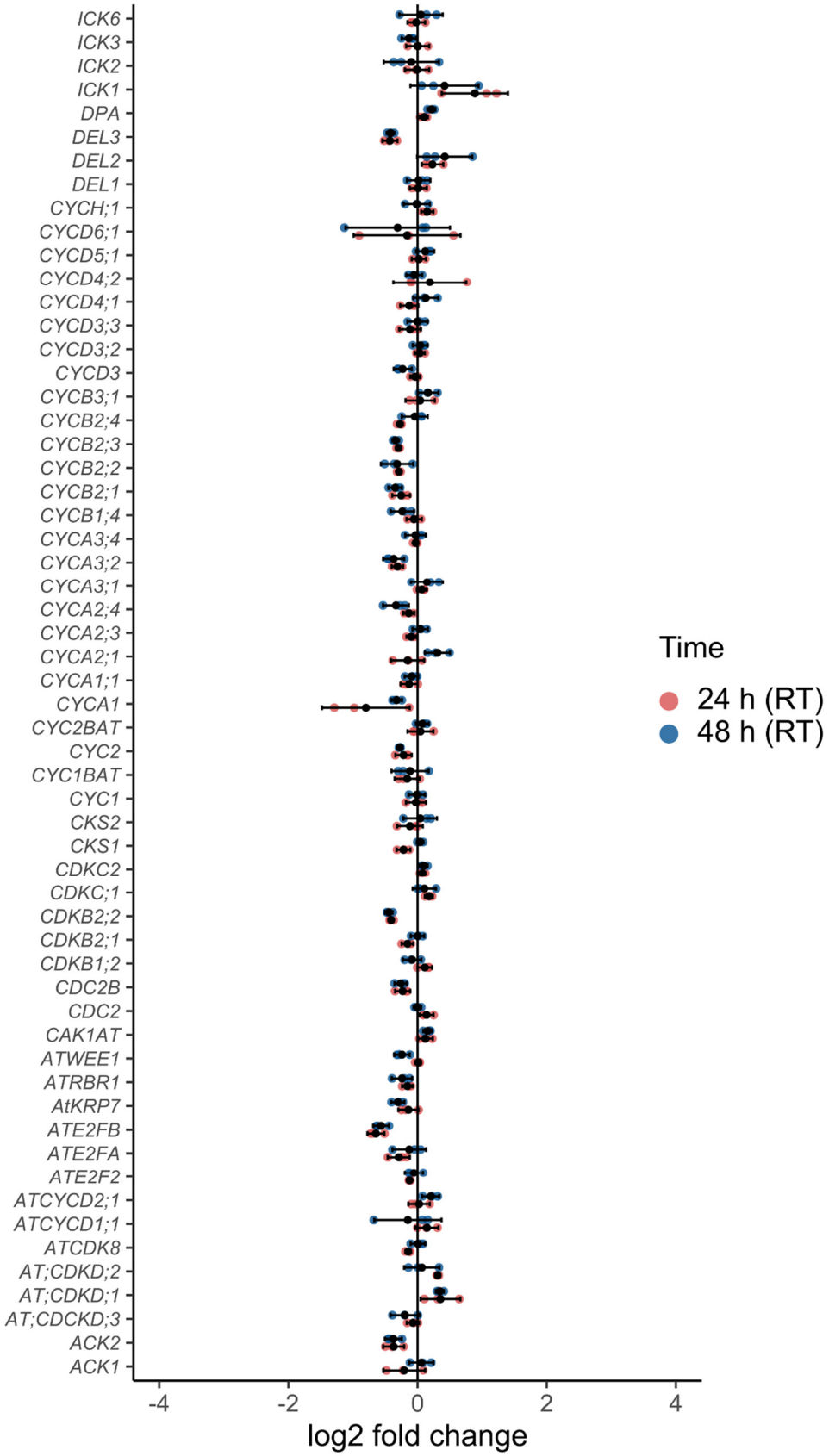

Supplementary Figure S7. Effect of 25 µM Cd on expression of cell cycle-related genes from Vandepoele *et al.*, (2002) in root tips (RT) after 24 h and 48 h. Values were obtained by dividing the DESeq2 normalized counts for each gene in the Cd-exposed sample by the mean of the respective control sample. Values are depicted as log2-fold changes.

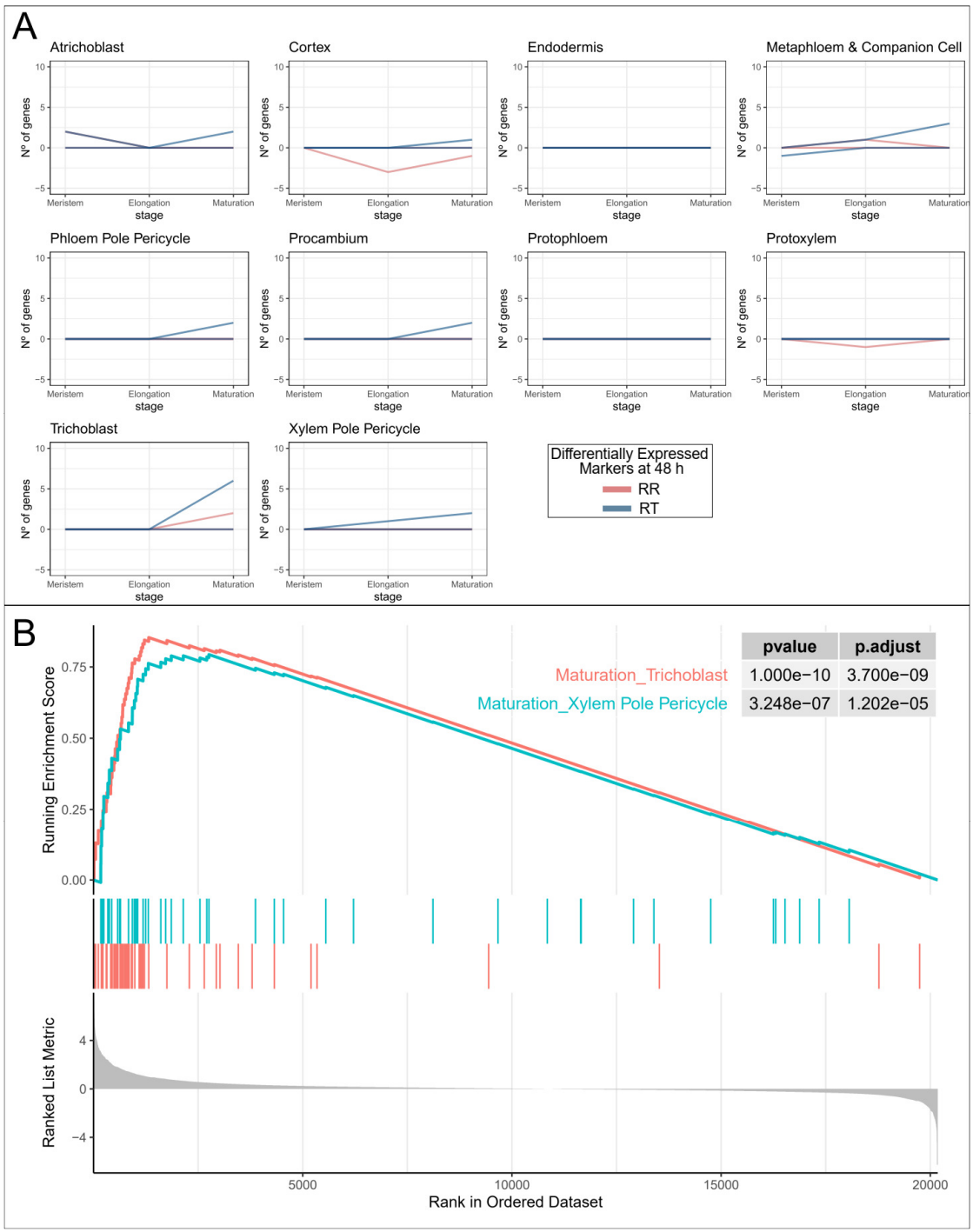

Supplementary Figure S8. Impact of Cd excess on differentiation in *A. thaliana* roots. Progression of the differentiation in the root tips upon Cd excess at 48 h. Bulk RNA-Seq data from root tip (RT) and remaining root (RR) samples upon growth in control or Cd treatments conditions were cross-referenced with the cell-type specific description of gene expression in roots provided by Shahan *et al.*, (2022). (**A**) Number of genes differentially expressed ($|\log_2$ fold change$| > 1$ and $p_{adj} \leq 0.05$) between Cd-treated and control samples that are among the 50 genes that are specific markers for each cell line and development stage. Positive and negative values in the Y-axis represent the number of DEGs that are upregulated or downregulated after Cd treatment, respectively. (**B**) Gene Set Enrichment Analysis of Developmental Markers. The plot shows the enrichment profiles of gene sets derived from Shahan *et al.*, (2022) between Cd-treated and control samples that were statistically significant (adjusted p-value < 0.05, Bonferroni correction).

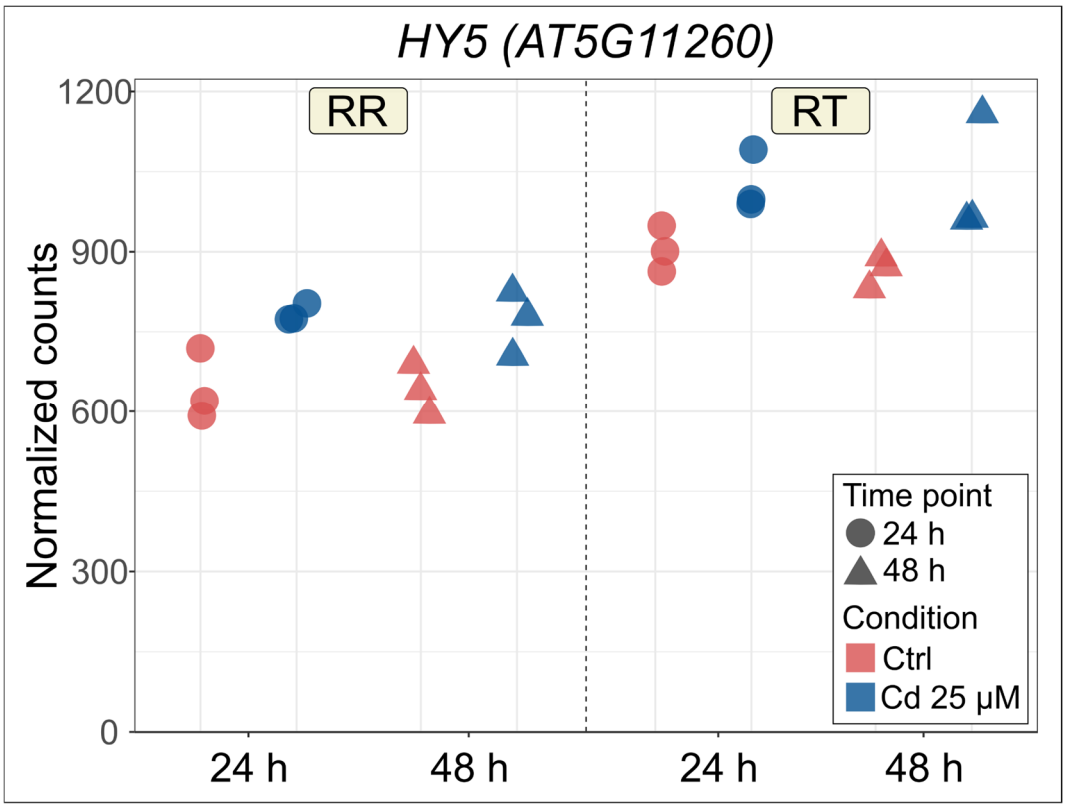

Supplementary Figure S9. Expression pattern of *HY5*. Normalized counts (DESeq2-processed) of HY5 transcripts in root tips (RT) and root rest (RR) under control conditions and after 24 h and 48 h Cd treatment. Individual data points represent biological replicates (n = 3).

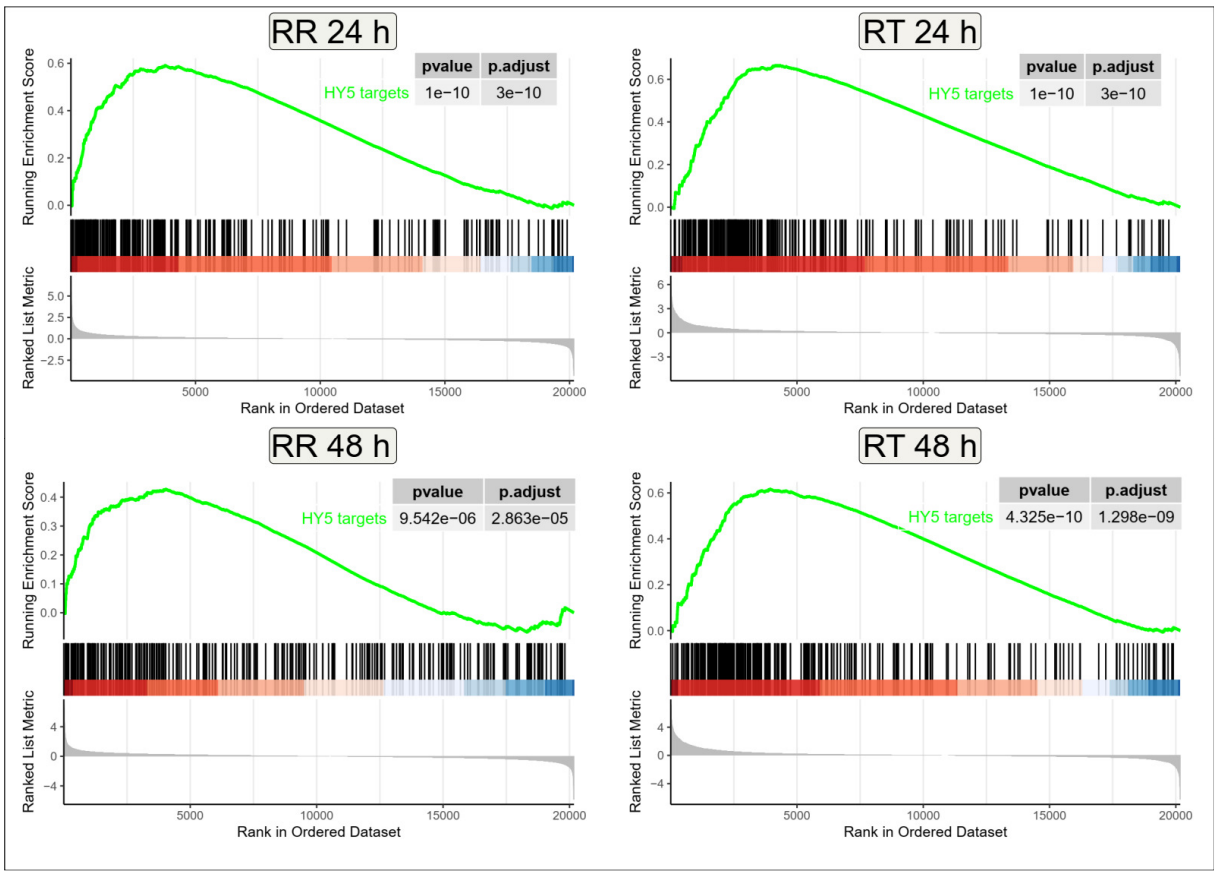

Supplementary Figure S10. Gene Set Enrichment Analysis of HY5 targets genes. The plot shows the enrichment profiles of HY5 target genes from Burko *et al.*, (2020) between control and Cd-treated samples (Adjusted p-value < 0.05, Bonferroni correction).

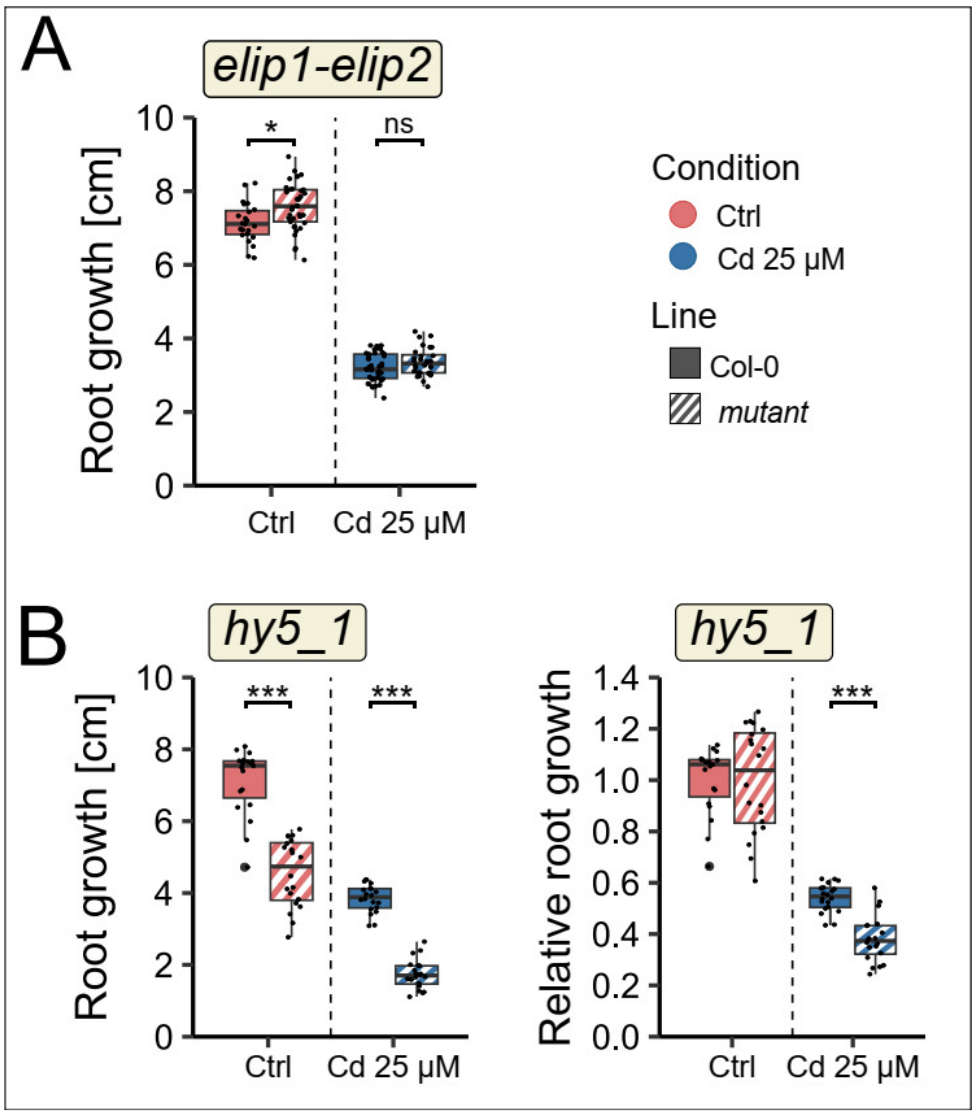

Supplementary Figure S11. Phenotypic analysis of root tip-responsive gene mutants under Cd stress. Primary root growth of *A. thaliana* mutants for candidate genes involved in the Cd response. Seedlings were grown for 7 days on control plates and then transferred to either control or Cd-containing plates for an additional 7 days. Asterisks denote statistically significant differences ($p \leq 0.05$, Mann-Whitney U-test; data from three independent biological replicates, n = 15–30 seedlings per replicate).

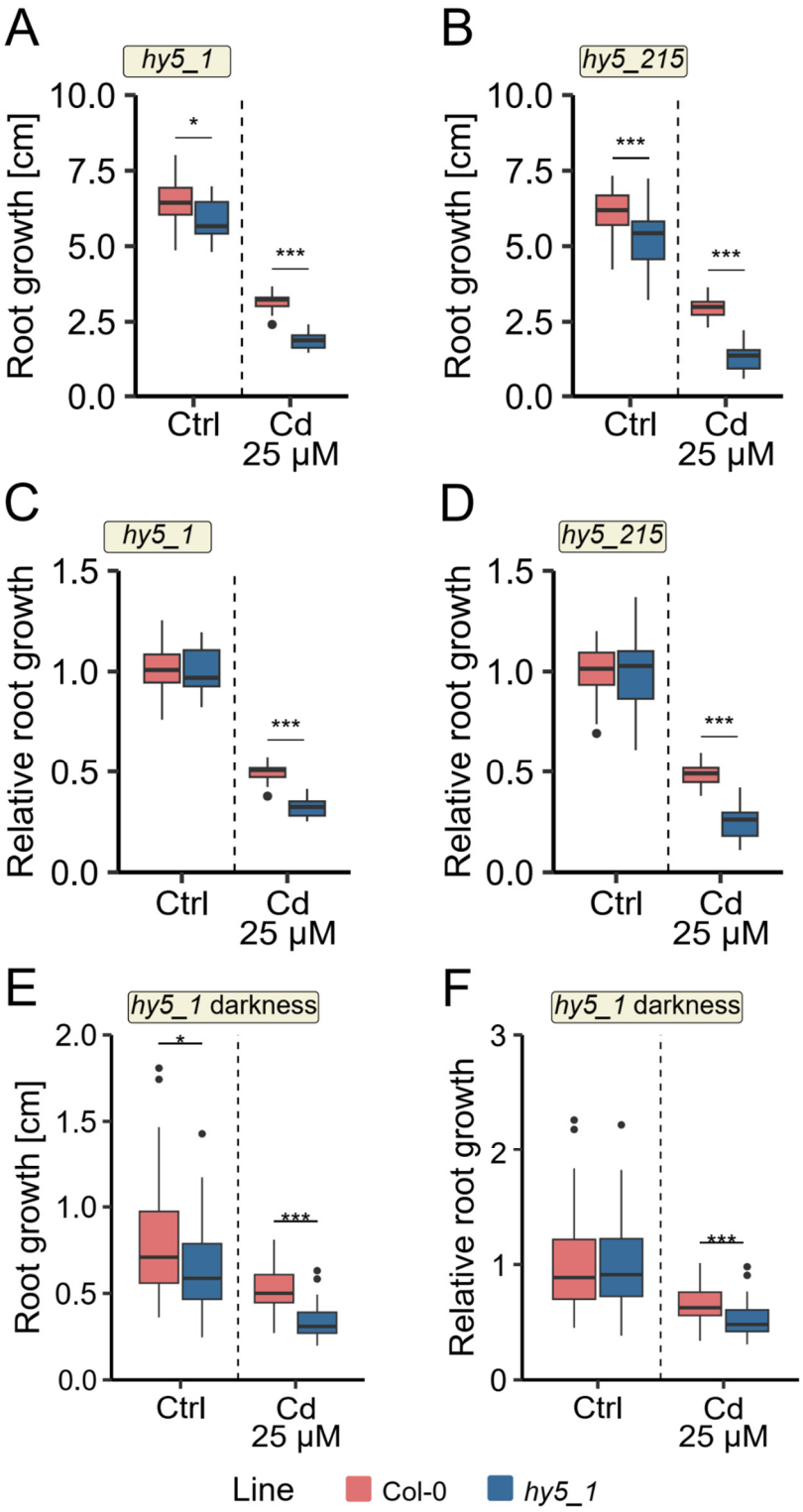

Supplementary Figure S12. Primary root growth of *hy5_1* and *hy5_215* under exposure to 25 µM Cd in a root covered system (A-D) and in darkness (E-F). Seedlings were grown on control medium for 7 d and then transferred to control or Cd medium and grown for additional 7 d. Values are depicted as absolute growth (**A-B**) and growth relative to the respective control (**C-D**). Asterisks indicate statistical significance (Mann Whitney U-Test, n=40-50, 3 independent replications, p≤0.05). (**E-F**) Primary root growth of *hy5_1* under exposure to 25 µM Cd in darkness. Seedlings were grown on control medium for 7 d and then transferred to control or Cd medium and grown for additional 7 d. Values are depicted as absolute growth (left) and growth relative to the respective control (right). Asterisks indicate statistical significance (Mann Whitney U-Test, n=37-43, 3 independent replicates, p≤0.05).

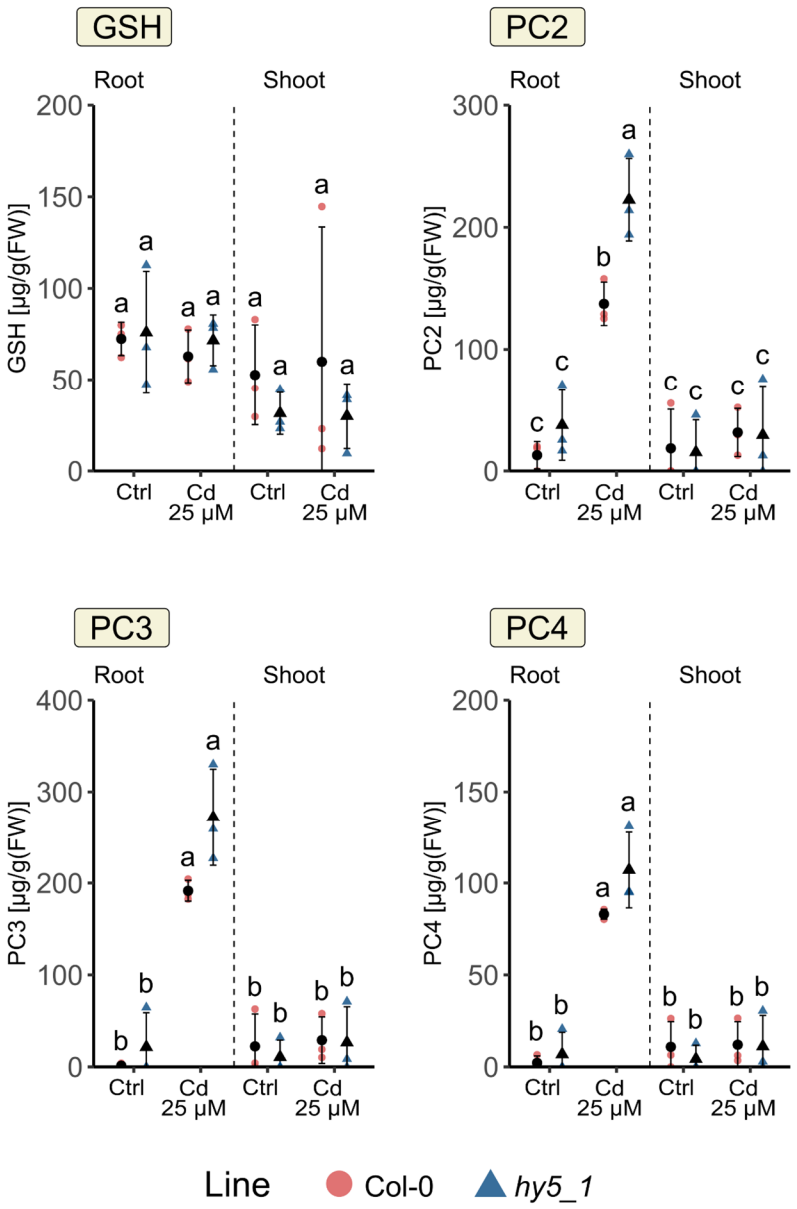

Supplementary Figure S13. Phytochelatin (PC) and glutathione contents in Col-0 and *hy5_1* upon exposure to 25 µM Cd. Seedlings were grown for 9 d on control medium and then transferred to control or Cd medium and exposed for 72 h. Displayed are mean values +/- standard deviations of contents in µg per gram fresh weight (FW). Letters indicate statistical significance (ANOVA with Tukey HSD, $p \leq 0.05$, data from three independent replications).

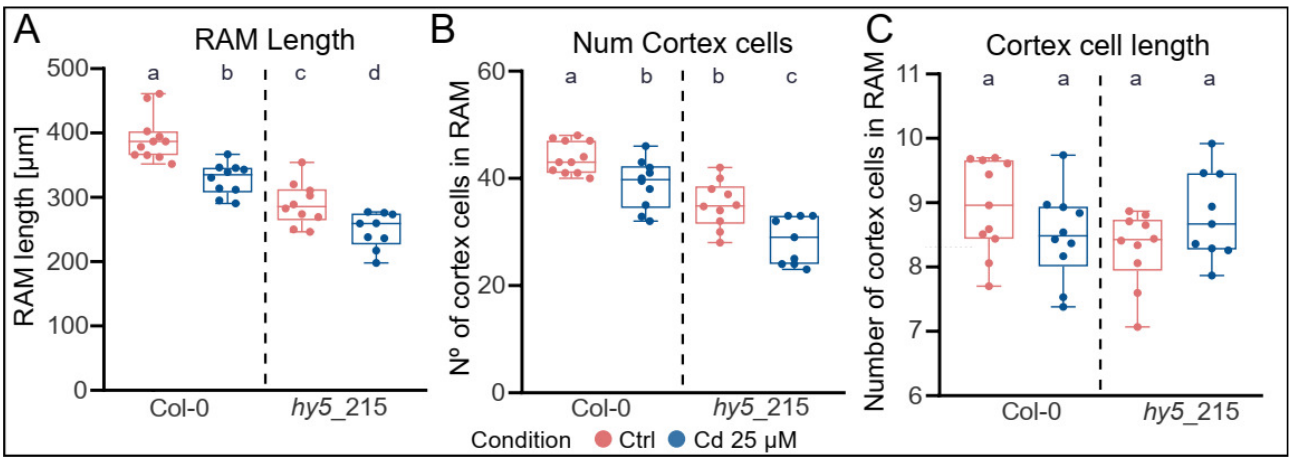

Supplementary Figure S14. **A** RAM size in Col-0 and *hy5* mutant lines. RAM size was defined as the distance from the quiescent center to the first elongated cortex cell. **B.** Number of cortex cells in the RAM. **C.** Cortex cell length. Cortex cell length was determined by dividing the length of RAM by the number of cortex cells in each meristem.Measurements originate from 9-11 seedlings per condition and time point (n=9-11) and one replication. Letters indicate statistically different groups (ANOVA with Tukey test, $p \leq 0.05$**)**.

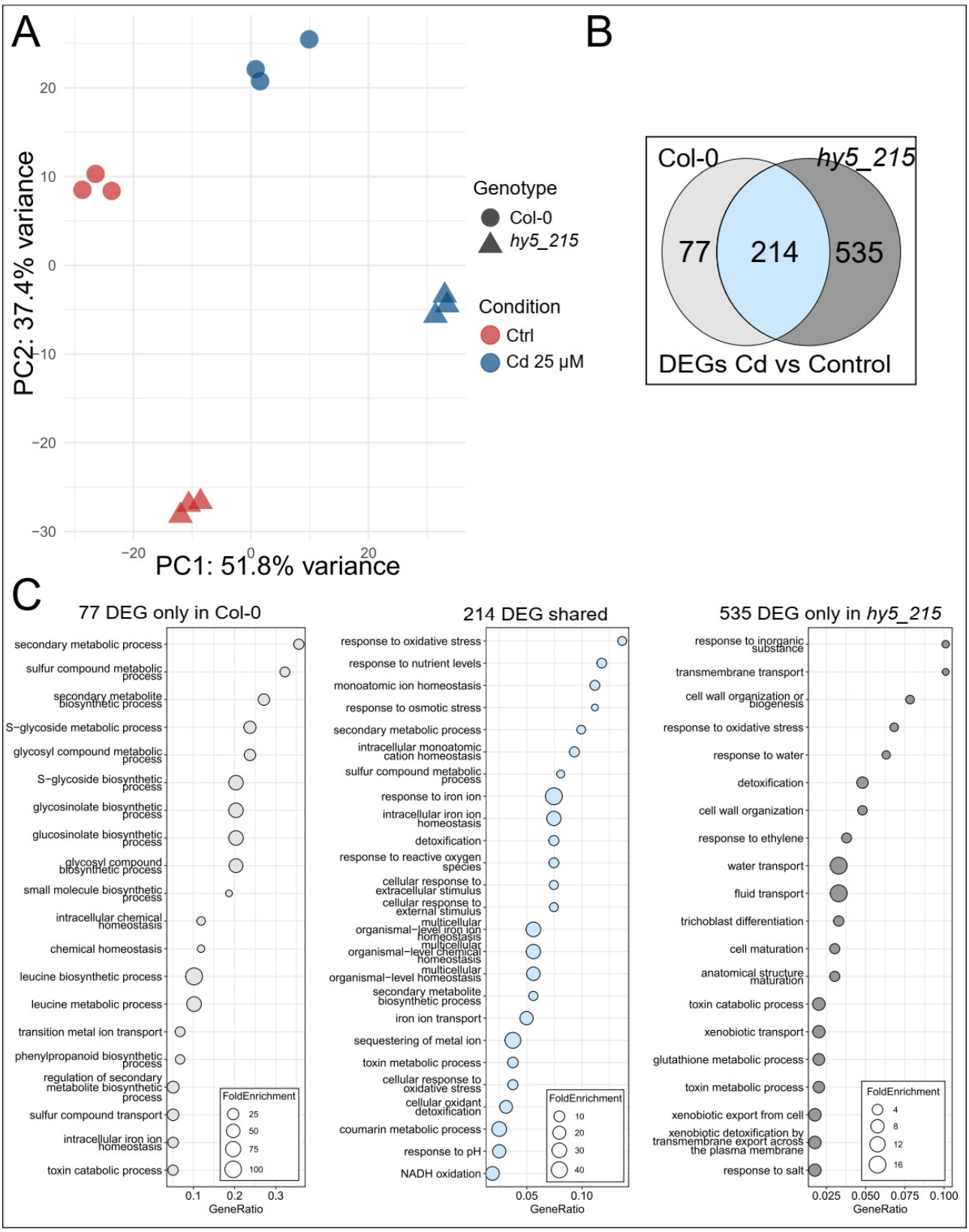

Supplementary Figure S15.Differential Expression Analysis in Col-0 and the *hy5_215* mutant using whole roots. **A.** Principal component analysis showing the distribution of samples according to PC1 and PC2. The percentage of variance explained by each PC is indicated in the corresponding axis. **B**. Venn diagram showing the number of DEG between Cd-treated samples and control**. C**. GO enrichment analysis for genes in B. The plots show the top GO terms with the lowest adjusted p-values (FDR), ordered by Gene Ratio (ratio of input genes that are annotated in a term). Circle size corresponds to fold enrichment.

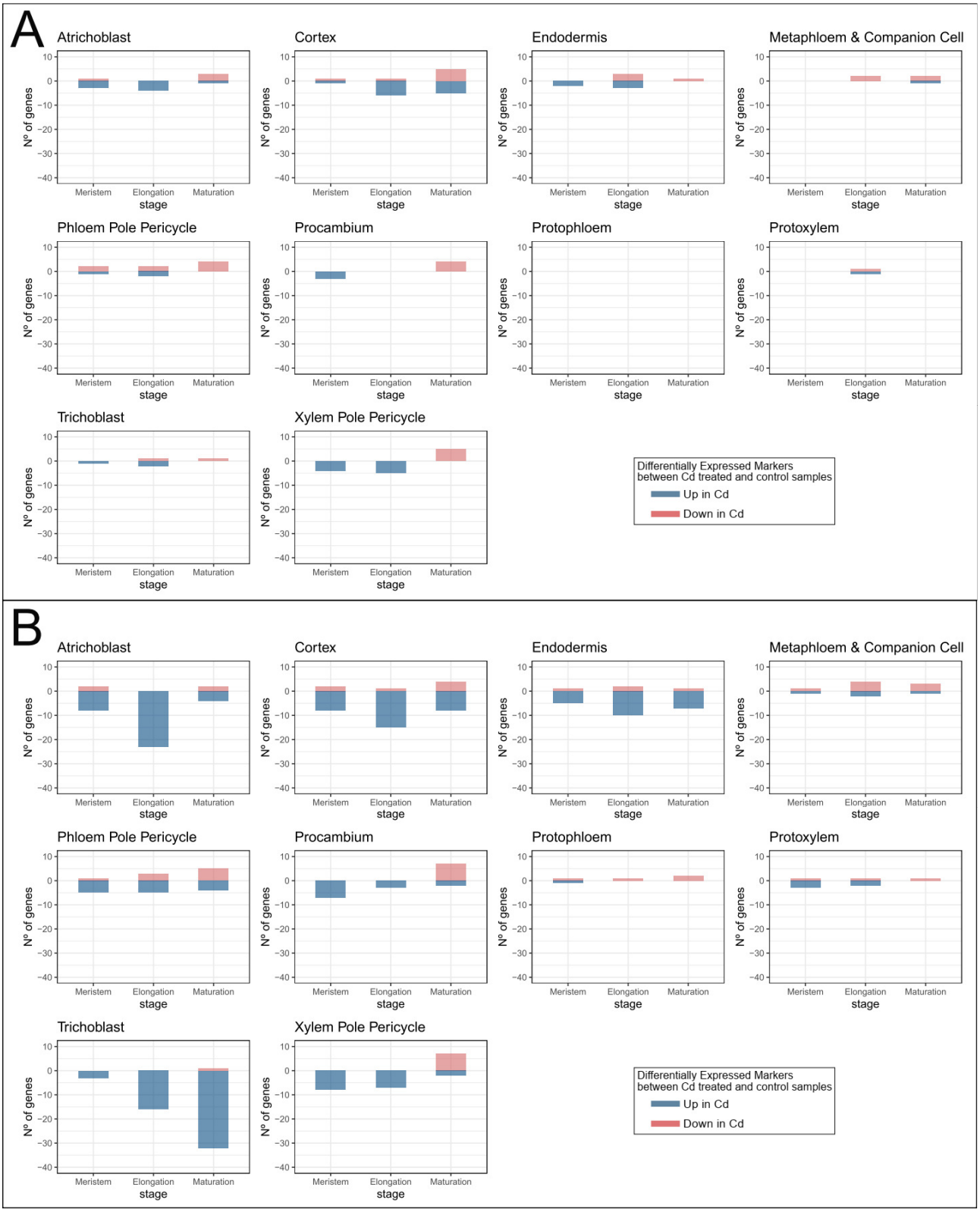

Supplementary Figure S16. Differentially expressed markers between Cd treated and control samples in the roots of *A. thaliana* Col-0 (A) and *hy5_215* (B) mutant. Bulk RNA-Seq data from whole roots samples upon growth in control and Cd conditions were cross-referenced with the cell-type specific description of gene expression in roots provided by Shahan *et al.*, (2022). Number of genes differentially expressed ($|\log_2$ fold change$|$ > 1 and $p_{adj} \leq 0.05$) that are among the 50 genes that are specific markers for each cell line and development stage. Positive and negative values in the Y-axis represent the number of DEGs that are upregulated or downregulated in Cd treated samples, respectively.

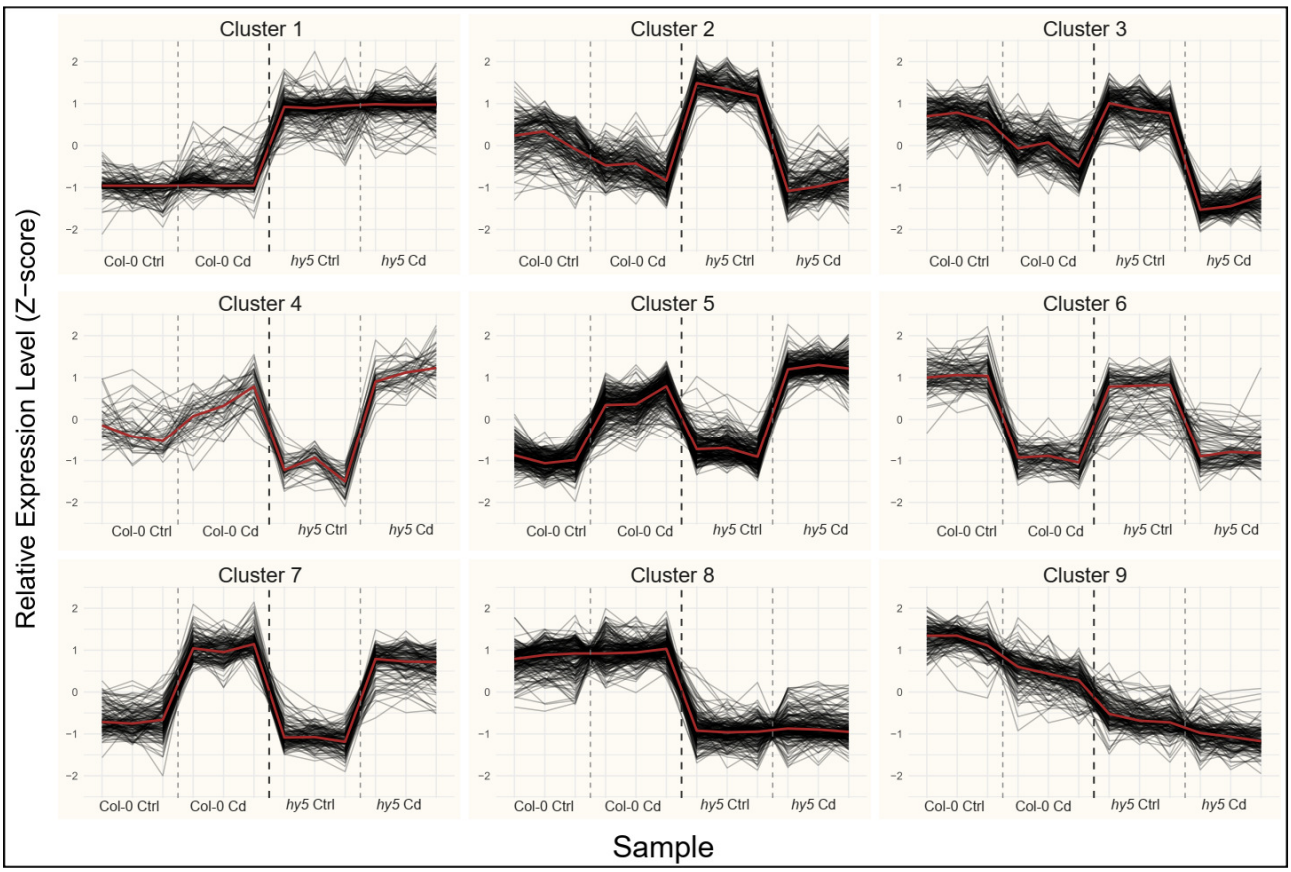

Supplementary Figure S17. Clustering and expression patterns of 1377 genes under Cd exposure in *Arabidopsis thaliana* Col-0 and *hy5_215* mutant roots. Self-Organizing Map analysis identified nine distinct gene expression clusters across four experimental conditions: (1) Col-0 control, (2) Col-0 Cd-treated, (3) *hy5* control, and (4) *hy5* Cd-treated samples, with three biological replicates per condition. Normalized expression data were obtained using DESeq2's variance stabilization transformation (VST), followed by Z-score normalization for each gene to minimize the influence of absolute expression levels on clustering. Line plots display individual gene expression patterns (black lines) and the median profile of each cluster (red line).

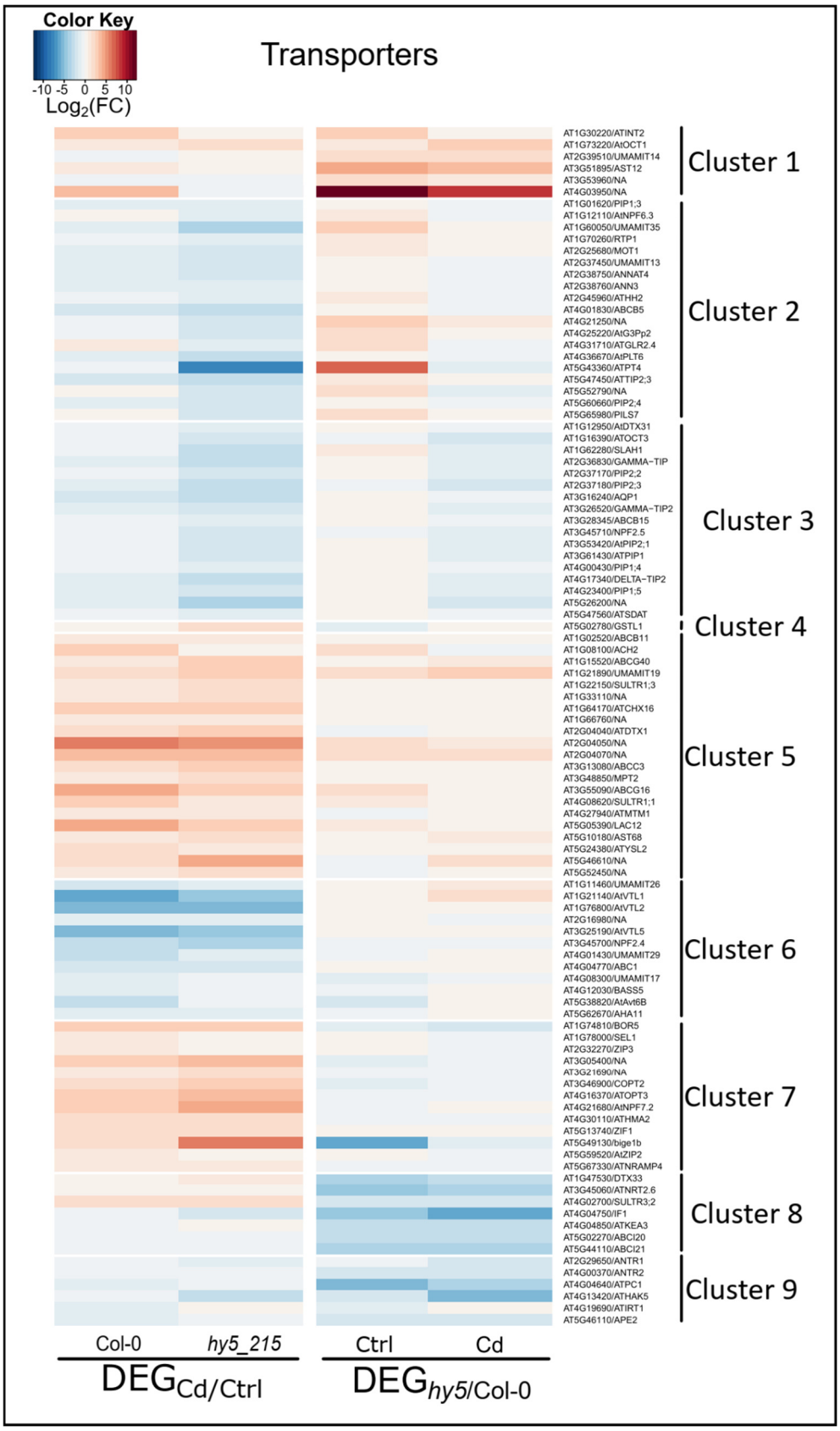

Supplementary Figure S18. Expression of transporter genes under Cd exposure in *Arabidopsis thaliana* Col-0 and *hy5_215* mutant roots. Using a list of predicted transporter genes from TransportDB, the heatmap shows the log2(fold change) of gene expression between conditions. In the $DEG_{Cd/Ctrl}$ columns, positive values indicate upregulation of genes after Cd treatment, while negative values indicate downregulation, in both Col-0 and *hy5_215* mutant roots after 48 h of treatment. In the $DEG_{hy5\_215/Col\text{-}0}$ columns, positive values indicate higher expression in *hy5_215* compared to Col-0, while negative values indicate higher expression in Col-0 compared to *hy5_215*.